

Available online at www.sciencedirect.com

jmr&t
Journal of Materials Research and Technology
journal homepage: www.elsevier.com/locate/jmrt



Review Article

Requirements for and challenges in developing improved creep ductility-based constitutive models for tempered martensitic CSEF steels



Raheeg Ragab ^{a,**}, Jonathan Parker ^b, Ming Li ^{c,***}, Tao Liu ^{a,*},
Andy Morris ^d, Wei Sun ^a

^a Faculty of Engineering, University of Nottingham, Nottingham, NG7 2RD, UK

^b Electric Power Research Institute, Charlotte, NC, USA

^c School of Mechanics, Civil Engineering and Architecture, Northwestern Polytechnical University, Xi'an, 710072, China

^d EDF Energy (UK), Coal Gas and Renewables, Central Technical Organisation, Barnwood, Gloucester, GL4 3RS, UK

ARTICLE INFO

Article history:

Received 11 November 2021

Accepted 8 February 2022

Available online 17 February 2022

Keywords:

Creep ductility

Cavitation

Continuum damage mechanics

Ductility exhaustion

Multi-axial stress state

CSEF steels

ABSTRACT

Creep fracture behaviour of tempered martensitic steels is generally governed by the process of cavity nucleation, growth and coalescence into microcracks. Therefore, creep ductility, which can be treated as material resistance to damage, has a critically important implication on the creep performance of materials and components, particularly where mechanical and metallurgical constraints are present. This review deals with some key aspects relating to creep ductility of high-temperature materials, paying a specific attention to creep strength enhanced ferritic (CSEF) steels. In the present work, the currently available state-of-the-art creep ductility-based constitutive models are reviewed, and the predictive capabilities of these models, particularly under multi-axial stress states, are examined. On this basis, the main limitations and challenges associated with using the existing models are evaluated and identified, and the requirements for developing improved creep ductility-based models for CSEF steels in order to carry out more accurate service life assessments are addressed.

© 2022 The Authors. Published by Elsevier B.V. This is an open access article under the CC BY license (<http://creativecommons.org/licenses/by/4.0/>).

* Corresponding author.

** Main Corresponding author.

*** Corresponding author.

E-mail addresses: raheeg.ragab@nottingham.ac.uk (R. Ragab), ming.li1@nwpu.edu.cn (M. Li), Tao.Liu@nottingham.ac.uk (T. Liu).
<https://doi.org/10.1016/j.jmrt.2022.02.047>

2238-7854/© 2022 The Authors. Published by Elsevier B.V. This is an open access article under the CC BY license (<http://creativecommons.org/licenses/by/4.0/>).

Nomenclature

Δ	Rupture elongation
Z	Reduction of area at rupture
L_0	Initial gauge length
L_u	Reference gauge length at rupture
A_0	Initial cross-sectional area of gauge section
A_u	Cross-sectional area at rupture
ϵ_{cu}	Uniaxial ductility
ϵ_{cu}^*	Multiaxial ductility
$\epsilon_{cu,loc}$	The true local strain at rupture
$\dot{\epsilon}_{min}$	Minimum creep rate
t_n	Time at void nucleation
t_f	Creep rupture life
ϵ'_{cu}	Intrinsic creep ductility
$\epsilon_{cu,m}$	Monkman-Grant ductility
f_h	Void area fraction
f_i	Void area fraction at nucleation
f_c	Void area fraction at coalescence
$\beta_{c,m}$	Void aspect ratio at failure under multiaxial stress state
μ	Stress triaxiality ratio
d_g	Grain size
ϵ'_p	A portion of the primary creep strain
λ	Damage tolerance factor
r	Notch root radius
d	The diameter at the minimum notch section
$\epsilon_{cu,u}$	Uniaxial creep ductility on Regime-I (upper shelf)
$\epsilon_{cu,l}$	Uniaxial creep ductility on Regime-III (lower shelf)
T	Temperature
σ	The applied stress
σ_m	Hydrostatic stress
σ_e	von Mises equivalent stress
σ_1	Maximum principal stress
$\dot{\epsilon}_c$	Creep strain rate
C_i	($i = 0, 1, 2, \dots$ etc) Material constants
$f(MP)$	Material Pedigree Function
n	Stress exponent at the secondary creep stage
m	Material constant accounting for the primary creep
p and q	Material constants in Spindler's ductility-based model
ω	Creep damage
CSEF	Creep Strength Enhanced Ferritic
BM	Base metal
WM	Weld metal
HAZ	Heat-affected zone
CTZ	Completely transformed zone
PTZ	Partially transformed zone
OTZ	Over tempered zone
CDM	Continuum damage mechanics
FE	Finite element

1. Introduction

Creep Strength Enhanced Ferritic (CSEF) steels with 9–12% Cr have been referred to as innovative high-temperature materials which are capable to cope with the increasing demand towards higher thermodynamic efficiency and reduced carbon emissions. Since their introduction, these materials have found increasing applications in various industrial fields, e.g., in power generation and petrochemical plants, owing to their superior high-temperature mechanical properties such as excellent creep strength, lower susceptibility to thermal fatigue and oxidation resistance [1,2]. Such properties are derived from the tempered martensitic microstructure, schematically shown in Fig. 1 [3]. The tempered martensitic microstructure in CSEF steels can be achieved by proper alloying as well as normalisation and tempering heat treatments to control the distribution and type of precipitates formed in the microstructure, and thereby maintain superior mechanical properties at high temperatures [3,4]. Details of heat treatment conditions for high chromium steels are documented in the cited reference [4]. The potential strengthening mechanisms in martensitic CSEF steels, resulting from alloying and heat treatment, are dislocation hardening, precipitation strengthening, and solid solution strengthening [4]. The microstructure of 9–12% Cr steels such as P91 and P92 steels typically exhibits a hierarchical arrangement, which can be subdivided into prior austenite grains (PAGs) consisting of packets, blocks and laths [3–6]. The

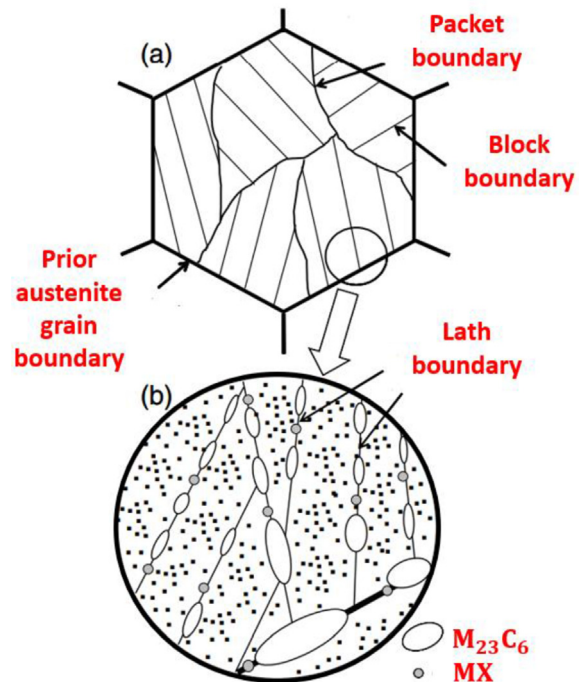


Fig. 1 – A schematic diagram showing the tempered martensitic microstructural features (PAG, packets, blocks, laths) and precipitate distributions of 9Cr–1Mo steel [3].

CSEF steels are also characterised by a fine dispersion of precipitates (e.g., MX carbonitrides and the Cr-rich $M_{23}C_6$ carbides) as well as high dislocation density [3–8].

Modern power generation plants are subjected to an ever-increasing range of temperature and pressure conditions [9,10]. As such, there appears an increasing need for improved computational constitutive material modelling to predict component performance with higher accuracy, and therefore, enhance plant efficiency and reliability. A number of creep and creep-fatigue damage models and life assessment methods have been proposed in recent decades (e.g. [11–21]). Based on material constitutive models, design methodologies for high-temperature structures have been established. However, it may be noted that the proposed design methods for pressure parts operating at high temperatures are generally based on uniaxial creep rupture strength data [22] while creep ductility, which is directly related to material resistance to damage, has received much less consideration. Creep ductility concerns on CSEF steels have been emphasised following the introduction of these materials into high-temperature power plants, where a range of operational and industrial challenges has been documented. For instance, the low ductility (damage tolerance) of the base metal was identified as one of the main causes for the premature heat-affected zone (HAZ) cracking observed in the welded joints of Grade 91 power plant headers [23,24]. Given the large variability observed in the creep performance of Grade 91 welded components, there have been increasing concerns that components fabricated from the steel casts, that exhibit poor creep ductility, may develop enhanced creep damage susceptibility under multi-axial stress states at positions where mechanical constraints due to poor design and metallurgical constraints due to material heterogeneity are present [25–27].

The significance of creep ductility and its influence on creep performance of materials at high temperatures have been further demonstrated in recent investigations. For instance, Siefert et al. [28,29] carried out an experimental study to link creep performance of CSEF steel weldments to the parent metal creep properties. It was shown that the low creep ductility of the base metal contributes to poor cross-weld creep performance and could lead to creep life reductions under multi-axial stress states [30,31]. This reduction can be generally related to creep damage being accelerated more rapidly than under a uniaxial stress state [31]. It is also believed that, at a longer term, the effects of creep ductility on creep crack growth and fracture behaviour of steels become more pronounced, possibly due to microstructural changes [32]. More specifically, a series of systematic microstructural investigations have been conducted [33–36] and a range of metallurgical risk factors have been elucidated in CSEF steels, which are generally linked to chemical compositions, microstructure, heat treatment, steel making practices and some other factors [27,31,37–39]. Such factors are found to influence creep cavitation behaviour in CSEF steels and increase the risk of fast fracture for low ductility steel casts [40–42]. Based on these findings, the link between creep ductility and the nucleation and growth of cavities is clear, which implies that creep damage constitutive models and design methodologies for structures fabricated from metallurgically susceptible steels such as CSEF steels should be based not only on creep

rupture strength but also on creep ductility. This is crucial to avoid the risk of catastrophic brittle failure due to the low damage tolerance of low ductility materials.

Several creep ductility-based models with different capabilities have been proposed to predict creep crack growth and damage in creeping solids (e.g., ref [43–48]). Although these models have provided reasonable predictions in some specific situations [49–51], their limitations to the application for the CSEF steels exist. The aim of this review is to provide a clearer picture of the role of creep ductility in high temperature structural integrity under multi-axial stress states. The paper is organised as follows: In Section 2, the concept of creep ductility and the current experimental methods adopted to measure creep ductility are reviewed. The key mechanical and metallurgical factors influencing creep ductility of CSEF steels are discussed in Section 3. In Section 4, the state-of-the-art uniaxial and multi-axial creep ductility-based models are reviewed. An appraisal of the existing creep ductility-based models is presented in Section 5, in which the capabilities of the state-of-the-art ductility-based models are examined, the main limitations of the models are identified, and on this basis, the requirements for future developments are addressed. Finally, a brief summary of this review is given in Section 6.

2. Creep ductility and experimental methods

2.1. Definition of creep ductility

It is generally established that, under a given stress state, the tendency for brittle type fracture in tempered martensitic CSEF steel is primarily controlled by the cavity growth and coalescence into microcracks [31,52,53], as demonstrated in Fig. 2, with damage rates being more enhanced under higher degrees of multi-axial stress states. On this basis, creep ductility may be generally defined as *the ability of a material to redistribute stresses and to avoid the propagation of a single crack* [32,54]. From metallurgical perspectives, creep ductility is related to the resistance of the material to cavitation damage [25,27,28,31]. As such, it is believed that creep ductility has a paramount influence on creep deformation and fracture

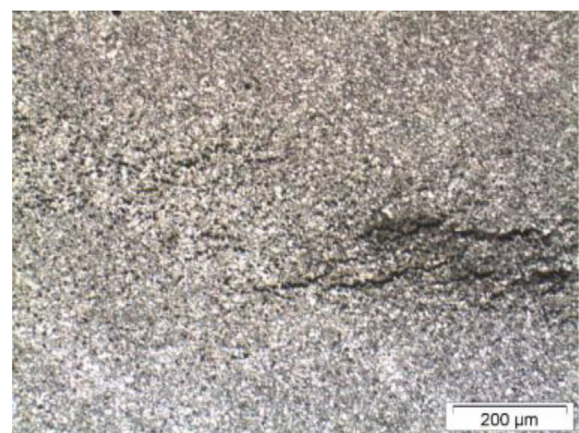


Fig. 2 – Micro-graph image showing microdamage and creep cavity formation in the HAZ of a P91 header weldment [24].

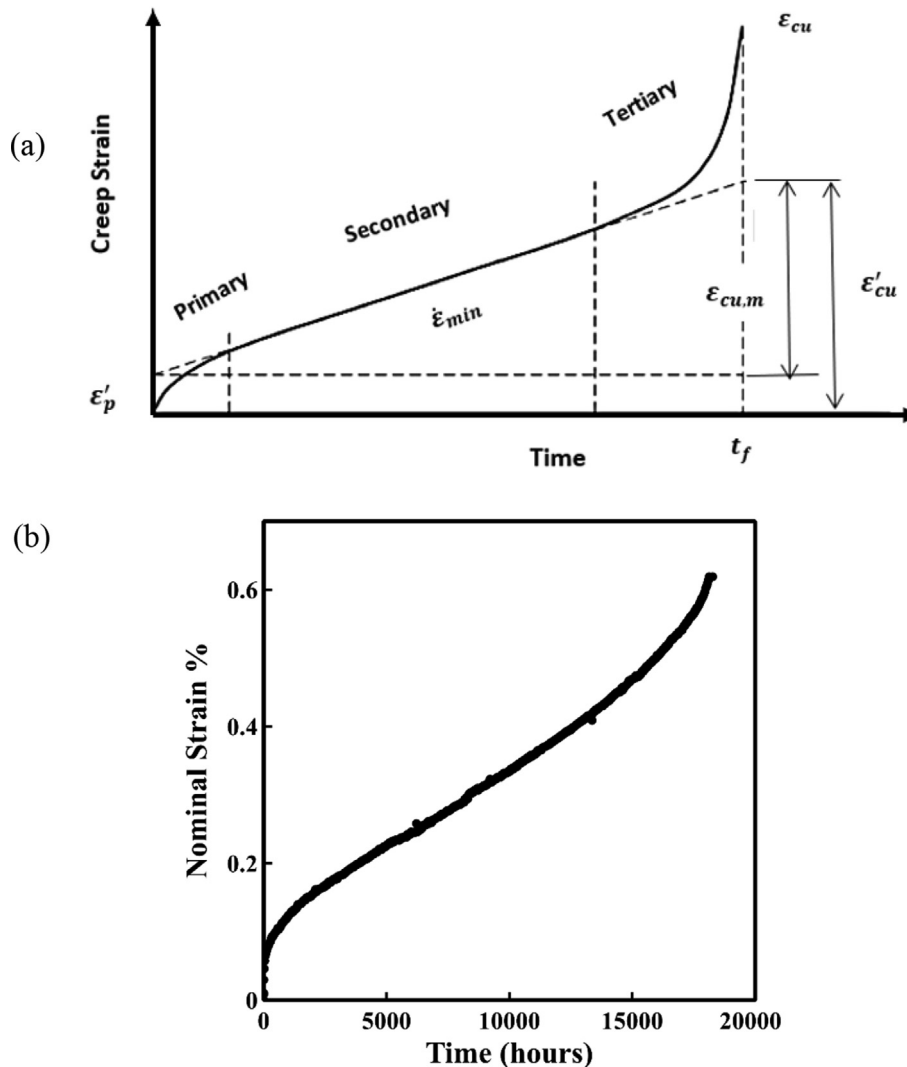


Fig. 3 – a) A schematic showing the stages of a typical creep curve in a constant load uniaxial test and some of the parameters characterising creep ductility (adapted from ref [32]), and b) Experimental data from a P91 cross-weld creep test at 625 °C and 60 MPa nominal stress [26].

behaviour of steels at high temperatures, particularly where mechanical notches due to poor design considerations and metallurgical constraints due to weldments are present [27,31]. In the following sections, the concept of creep ductility is further elaborated for uniaxial and multi-axial stress states.

2.1.1. Uniaxial creep ductility

Figure 3a depicts schematically a typical three-stage uniaxial creep curve, comprising primary creep, secondary creep and tertiary creep. It may be noted that under some conditions there may be very limited primary creep and in other cases the tertiary creep component is dominant. The primary creep stage is characterised by decreasing creep strain rates with time due to strain hardening [55]. During the secondary or steady-state creep, the rate of strain hardening is balanced by the rate of thermal softening [56], leading to a constant or minimum creep strain rate, $\dot{\epsilon}_{min}$. The tertiary stage represents a region of accelerating creep strain rates due to thermal softening until rupture occurs. This stage of creep is also often

associated with microstructural instability and metallurgical changes such as substructure recovery [57], the formation of new phases [58], coarsening of existing precipitates [59] and accumulation of damage due to cavitation and microcracks [55]. Figure 3b depicts the creep curve of a long-term feature type cross weld creep test at nominal stress of 60 MPa, which has a general shape to that shown in Fig. 3a.

An important parameter that can be evaluated from the uniaxial creep curve, Fig. 3a, is the uniaxial creep ductility, which can be considered as *a measure or an indicator of the susceptibility of a given material to creep damage under a uniaxial stress state condition*. Figure 3a shows a schematic of the nominal creep strain vs time in a constant load uniaxial creep test. The uniaxial creep ductility can be characterised through a number of parameters as illustrated below.

The most used parameters to characterise uniaxial creep ductility are creep rupture elongation and reduction of cross-sectional area at rupture, which are expressed by Equations (1) and (2), respectively:

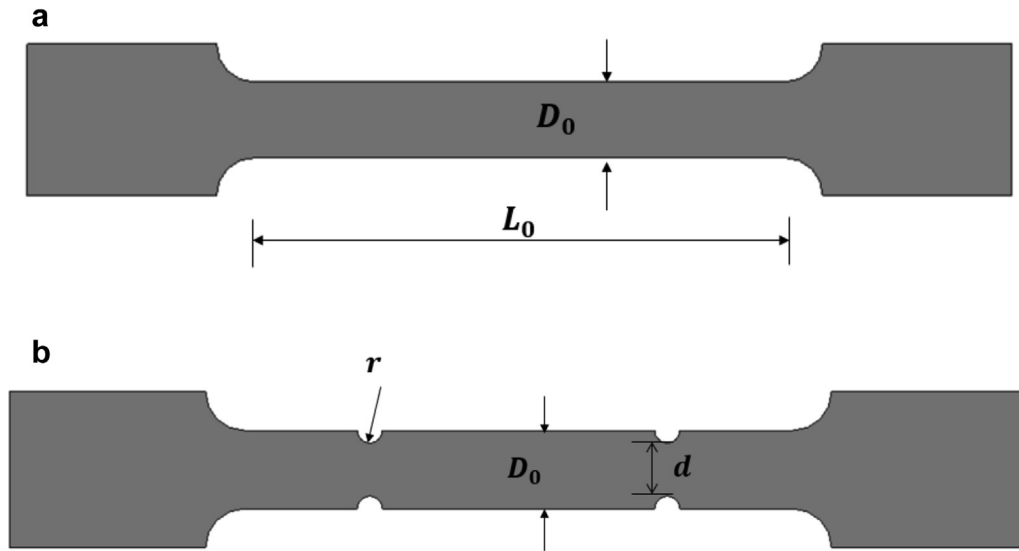


Fig. 4 – a) A schematic diagram of the plain bar uniaxial specimen (L_0 denotes the gauge length and D_0 is the diameter of the smooth bar). b) A schematic diagram of the notched bar specimen with double notches (d denotes the diameter of the notch throat while r represents the notch root radius).

Creep rupture elongation, Δ , is given by:

$$\Delta = \frac{L_u - L_0}{L_0} \quad (1)$$

Reduction of area at rupture, Z , is given by:

$$Z = \frac{A_0 - A_u}{A_0} \quad (2)$$

where L_0 and L_u are the initial gauge length and gauge length at rupture, respectively. A_0 and A_u denote the initial cross-sectional area of gauge section and cross-sectional area at rupture, respectively. Alternatively, if the initial instantaneous strain upon loading is insignificant, the rupture elongation (Δ) can be assumed as an equivalent to creep strain at rupture, ϵ_{cu} [32].

In previous investigations (e.g., refs [49,50]), creep rupture strain and reduction of area at rupture were used to represent the uniaxial creep ductility and have shown to be able to predict creep failure with reasonable accuracy.

Creep ductility can also be expressed in terms of the true local strain at rupture, $\epsilon_{cu,loc}$, as illustrated below:

$$\epsilon_{cu,loc} = \int_{L_0}^{L_u} \frac{dL}{L} = \ln(L_u) - \ln(L_0) = \ln\left(\frac{L_u}{L_0}\right) \quad (3)$$

Using the constant volume assumption (incompressibility) of plastic flow, we have:

$$A_0 L_0 = A_u L_u \text{ or } \frac{L_u}{L_0} = \frac{A_0}{A_u} \quad (4)$$

Substituting Equation (4) in (3) yields the following expression for creep ductility in terms of the true local strain at rupture:

$$\epsilon_{cu,loc} = \ln\left(\frac{1}{1-Z}\right) \quad (5)$$

Although the above parameters are widely adopted to characterise creep ductility of materials for their convenience and

the ease with which they can be determined experimentally (e.g. based on uniaxial creep rupture tests), they are known to depend on the size of the tested specimens [32,60]. To overcome these challenges, some practical indicators to represent creep ductility are proposed such as the intrinsic creep ductility, ϵ'_{cu} , and Monkman-Grant ductility [61], $\epsilon_{cu,m}$, as defined in Fig. 3. The intrinsic creep ductility, ϵ'_{cu} , is assumed to comprise two components as given by Equation (6), while the Monkman-Grant ductility, $\epsilon_{cu,m}$, is given by the product of the minimum creep rate ($\dot{\epsilon}_{min}$) and creep rupture life (t_f), as expressed by Equation (7).

$$\epsilon'_{cu} = \epsilon'_p + \epsilon_{cu,m} \quad (6)$$

$$\epsilon_{cu,m} = \dot{\epsilon}_{min} t_f \quad (7)$$

As illustrated by Equation (7) and Fig. 3, the Monkman-Grant ductility, $\epsilon_{cu,m}$, ignores a significant portion of the primary creep strain and also the tertiary creep. Therefore, this parameter will only provide a reasonable approximation of the intrinsic creep ductility if the primary creep strain is sufficiently small ($\epsilon'_p \approx 0$) and steady-state creep is dominated. While creep ductility is typically measured in terms of creep rupture strain or reduction of area at rupture, the Monkman-Grant ductility is thought to provide a relatively more accurate representation of creep ductility since it can be considered as a measure of the local strains produced by the creep diffusional processes occurring uniformly at the microstructural/grain-boundary levels prior to any necking [45].

Based on Equations (6) and (7), another important ductility parameter can be introduced, known as creep ductility ratio or damage tolerance factor, λ , as given by Equation (8). This parameter provides useful insights about the capacity of steels to redistribute stresses in structural components [32,54] and can also be used as an indicator to assess material susceptibility to localised cracking at strain concentrations [38,62]. For instance, based on this parameter, it has been

Table 1 – A summary of the common notched bars geometry, materials and creep test conditions.

Notch acuity ratio (d/r)	Material	Temperature ($^{\circ}\text{C}$)	Net section stress (MPa)	Rupture life (hours)	Reduction of area (%)	Reference
0	P92	650	145	403.3	92.16	[82]
2.8				1083.8	23.06	
20				1203.3	2.27	
0	9Cr–1Mo	600	150	63.55	90	[76]
1				163.1	86.71	
2				537.80	64.86	
4				943.10	45.87	
10				1452.20	17.08	
20				1200	13.37	
0	9Cr–1Mo	600	210	3.5	93.37	[77]
1				18.6	87.58	
2				22.75	82.65	
4				65.9	75.79	
10				89.1	61.60	
20				120	50.16	
0	FB2	605	350	5.1	70.62	[79]
10				988.8	4.97	
24				1212.1	4.26	

proposed that steels can be classified into creep ductile ($\lambda \geq 5$) and creep brittle ($\lambda < 5$) [38]. However, these boundaries have not been evaluated for a wide range of alloys nor stress states.

$$\lambda = \frac{\epsilon_{cu}}{\epsilon_{cu,m}} \quad (8)$$

where ϵ_{cu} is the creep strain at rupture.

2.1.2. Multi-axial creep ductility

Multiaxial creep ductility may be regarded as an indicator to the resistance of a given material system to creep damage when subjected to a multi-axial loading condition. It is believed that under multi-axial stress state conditions, voids growth rate becomes higher [15] and therefore, creep ductility under multi-axial loading conditions is typically lower [15,32]. This reduction can significantly influence creep behaviour of steels and consequently lead to creep damage and early fracture. The multi-axial creep ductility can also be characterized in terms of creep rupture elongation or reduction of area as measured from bi-axial notched bar creep rupture tests. Alternatively, the multiaxial creep ductility can be computed based on the uniaxial creep ductility through implementation of void growth models such as Rice-Tracey [63] and Cocks-Ashby models [64], as illustrated in further details in Section 4.

2.2. Experimental methods to measure creep ductility

2.2.1. Uniaxial creep tests

Conventional uniaxial creep tests are often conducted on plain bars, as shown schematically in Fig. 4a, to study creep deformation and fracture behaviour of engineering materials under uniaxial stress state. The experimental tests are typically conducted following standard methods, e.g. ASTM E139 [65] and BS EN 10291 [66]. In these tests, constant force is usually applied at a constant temperature and the corresponding deformation with time (i.e., creep curve) is monitored during the test. The typical creep curve obtained from such tests is shown schematically in Fig. 3, which can provide

useful information on creep deformation and damage properties. The uniaxial creep ductility can be evaluated from uniaxial creep tests as the engineering creep strain at failure (ϵ_{cu}) or in terms of the reduction of area %.

In addition to the standard uniaxial creep tests, small-scale creep testing techniques such as impression creep test, small punch creep test and other miniature specimen testing techniques have received increasing attention because they require small volumes of materials to be sampled [67,68]. The two-material miniature specimen test method proposed by [67] can reasonably characterise the tensile and creep properties of materials. One of the key advantages offered by such a test is that it can reproduce the full uniaxial creep curves from a very small volume of material [67]. Therefore, creep ductility may be obtained from this test in a similar manner to that in conventional uniaxial creep tests. However, it should be noted that the size dependency, surface oxidation etc can be considered as potential limitations of the application of small-scale testing techniques to measure creep ductility which generally requires a sufficiently long creep time.

2.2.2. Multi-axial creep tests

Multiaxial creep ductility is usually determined by notched bars creep rupture tests at high temperatures. The introduction of notches, which can be of different shapes and geometries, into creep specimens imposes local constraints on creep deformation and results in a significant level of multi-axial stress state. Such tests can be carried out on either single or double notched bars, shown in Fig. 4b, with the latter being preferred as they enable examination of the state of damage in the material close to rupture through the unbroken notch [69]. In notched bar creep tests, the multiaxial creep ductility is typically measured in terms of reduction of area % rather than elongation at rupture since the axial strain is not uniform over the gauge length [70].

Other techniques for characterising the multi-axial creep behaviour include cruciform specimens under biaxial tension

creep loading [71,72], thin-walled tubes under pure torsion [73], thin-walled tubes subjected to combined tension and torsion [74], pressurised tubes and pipes under creep loading [75], which are thought to be more representative of stress states in real components. All these tests can provide useful insights into the stress state effects on creep damage and fracture and how stresses redistribute during creep.

3. Factors influencing creep ductility

Creep ductility can be influenced by a range of mechanical and metallurgical variables. In practice, the mechanical variables relate to plant operation and installation and involve, for example, stress state, stress level, strain rate and pre-straining, while the metallurgical factors are related to steel manufacture and fabrication practice including chemical composition and microstructure, material heterogeneity, steel fabrication methods, and heat treatment conditions. These factors will be reviewed in more details in the following subsections to gain insights into their effects on creep ductility and to fully appreciate their key role when developing improved creep ductility-based models for CSEF steels.

3.1. Mechanical constraints

3.1.1. Effects of stress state

In practice, pipes and tubes under internal pressure are typically operating under multi-axial stress conditions. The local stress state will be further complicated by a sudden change in geometry (mechanical or thermal) loading conditions or material properties such as the introduction of weld joints. It has been widely reported that the exhaustion of creep ductility under multi-axial stress state is responsible for the generation of in-service creep damage [32]. As such, it is very important to fully understand the effect of stress state on creep ductility. The influence of stress state on creep ductility can be investigated experimentally using multi-axial creep tests such as notched bar creep rupture tests. Several studies have examined the influence of stress state on creep ductility and damage using experimental notched bar rupture tests (e.g., ref [76–80]). Table 1 provides a summary of the common notched bars

geometry, materials and creep test conditions reported in the literature. The relevant experimental findings are also reviewed and listed in Table 1 and presented in Fig. 5. The notch acuity ratio, d/r , in Table 1 refers to the ratio of the notch throat diameter, d , to notch root radius, r , as illustrated in Fig. 4b. This ratio controls the degree of stress state and hence the multi-axial creep ductility. As illustrated in Table 1, the notched bar specimens under creep conditions exhibit notch strengthening effect, i.e., the rupture life of the notched bar is higher than that of the plain bar ($r \rightarrow \infty$) with notch acuity ratio $d/r = 0$. It is usually the case that tests of short duration show notch strengthening, however in some alloys notch weakening has been observed in long duration tests. The general trend of experimental rupture ductility shown in Table (1) and Fig. 5 does suggest that creep ductility (in terms of reduction in area at rupture) tends to decrease with the introduction of notches, which becomes more pronounced with the increase in the degree of constraint (i.e., higher notch acuity ratios). Figure 5 also indicates that creep ductility is high at high stresses and low at low stress regime. Experimental investigations have demonstrated that as creep ductility decreases, due to an increase in the degree of constraint, the fracture surface appearance of the notched bars tends to change from ductile transgranular to brittle intergranular fracture dominated by creep cavitation [77,81,82], as illustrated in Fig. 6. The brittle fracture mode observed in accelerated notched bar tests under specific conditions is analogous to that observed in service, where low ductility failure of components is usually associated with the presence of high density of cavitation [27]. The transition in fracture behaviour could be explained in part by the shift from von Mises controlled fracture to maximum principal stress dominated failure [76,77].

3.1.2. Effects of creep strain rate

The effect of creep strain rates on creep ductility of materials is a complex process as it involves several creep damage and fracture mechanisms. Hales [83] proposed three creep regimes to characterise the variation of creep rupture ductility with strain rates, namely i) Viscoplastic cavity growth regime (Regime-I), ii) Diffusion controlled cavity growth regime (Regime-II), and iii) Constrained cavity growth regime (Regime-III), as shown schematically in Fig. 7a. Regime-I (Upper Plateau) is characterised by high strain rates and high rupture ductility since the fracture process is dominated by plasticity controlled void growth, as presented in Fig. 7b. Regime-II (transition region) shows a remarkable drop in creep ductility with the decrease in strain rates. In this regime, the cavitation rate is controlled by the rate of vacancy diffusion on the grain boundary and the grains are assumed to be rigid, Fig. 7c. In Regime-III (Lower Plateau) with low strain rates, the rate of cavitation is constrained by the slow creep deformation of the matrix and grain boundary sliding, resulting in lower creep ductility, Fig. 7d. As shown, creep ductility in the lower plateau (Regime-III) is insensitive to strain rates. This regime description is found to be consistent with the experimentally measured creep rupture data of 1CrMoV steel at 500 °C [84], Type 304 steel at 593 °C [85] and 1CrMoV rotor steel at 550 °C [60], as illustrated in Fig. 8a, Fig.8b and Fig.8c, respectively. Generally, the data show the first two regions whereas the evidence for Regime-III is limited.

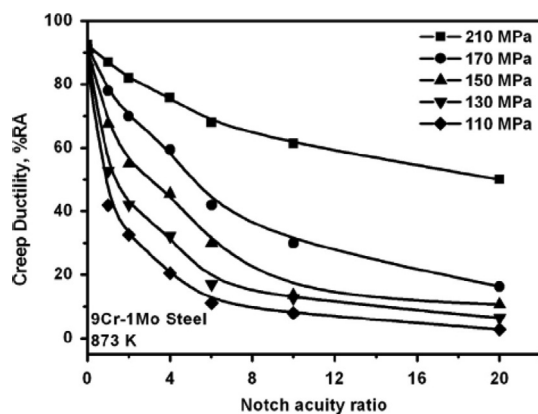


Fig. 5 – Influence of degree of constraint (notch acuity ratio) on creep ductility parameter (reduction of area %) for 9Cr–1Mo steel at 873 K [77].

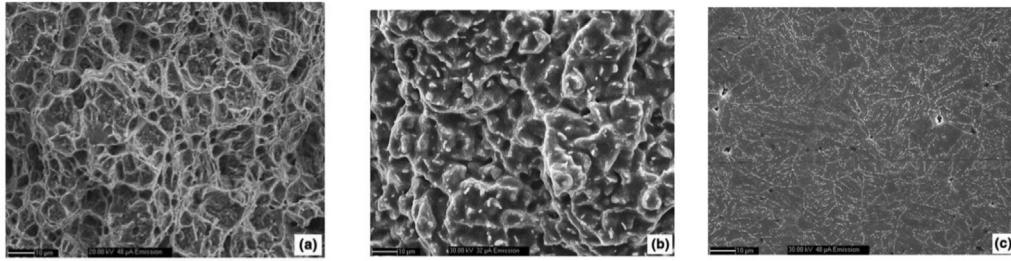


Fig. 6 – SEM micrographs showing: (a) ductile transgranular dimple failure observed in the notched bar with $d/r = 4$ (at central region), (b) brittle intergranular fracture in the notched bar with $d/r = 20$ (at notch root), and (c) creep cavitation at notch root for the notched bar with $d/r = 20$ (Creep tests under stress of 150 MPa at 600 °C) [76].

3.1.3. Effects of stress levels

It has been experimentally observed that creep ductility is high at the high-stress (accelerated creep) regime and low at low stresses (long-term creep regime), as shown in Fig. 9a. This is also consistent with the creep deformation regime proposed by Hales [83] and shown in Fig. 7. The general features characterising ductile and brittle fracture in 9%Cr steel plain bars (tested under creep conditions) are illustrated in Fig.9b and Fig.9c. As shown, the ductile fracture observed in plain bars tested at higher stress levels (Regime I) is associated with a high degree of necking, while the brittle fracture in plain bars tested under lower stress levels (Regime III) is characterised by reduced necking, i.e., lower ductility.

Another splitting regime to characterise the variation of creep ductility over short-term and long-term creep is proposed by Holdsworth [32] and shown in Fig. 10a. Compared to that of Hall [83], the splitting regime shown in Fig. 10a consists of four creep rupture stages [32]. Regime-I (at high stresses) exhibits relatively high rupture ductility with ductile-transgranular rupture due to the formations of voids caused by particle/matrix decohesion. In Regime-II (transition region) a significant drop in creep ductility due to the increased grain boundary cavitation and matrix deformation is evident. At relatively lower stress values, Regime-III, ductility reaches its lowest values due to the nucleation and diffusive growth of cavities at the grain boundaries. Holdsworth [32] argued that

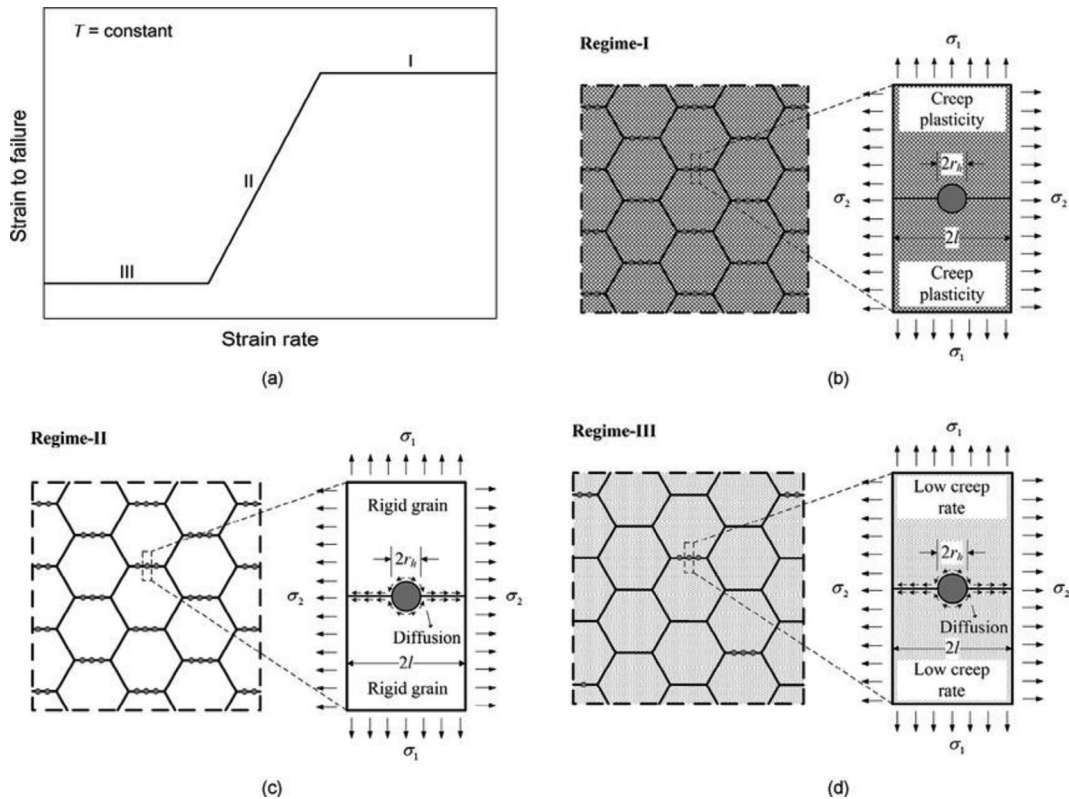


Fig. 7 – Schematic representation of the effect of strain rate on creep rupture ductility [70]: (a) The three regimes proposed by Hales [83]; (b) Regime-I: viscoplastic cavity growth; (c) Regime-II: diffusion-controlled cavity growth; and (d) Regime-III: constrained diffusion cavity growth.

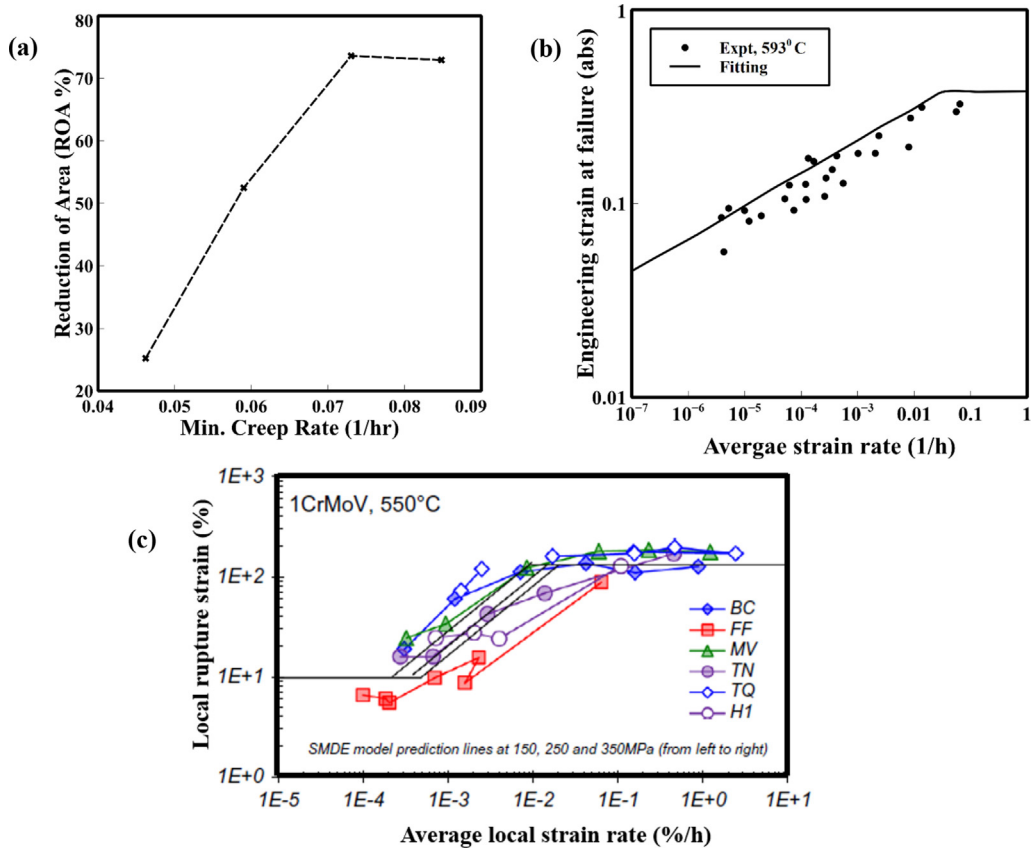


Fig. 8 – Experimental creep rupture data showing dependency of creep ductility on strain rates for different steel grades. a) creep ductility variation in terms of reduction of area at rupture against minimum creep rate for 1CrMoV steel at 500 °C [84], b) variation of creep ductility (defined as engineering strain at failure) for Type 304 steel at 593 °C [85], and c) variation of local rupture strain % for 1CrMoV rotor steel at 550 °C (BC, FF, MV, TN, TQ, H1 are steel heats with different chemical compositions) [60].

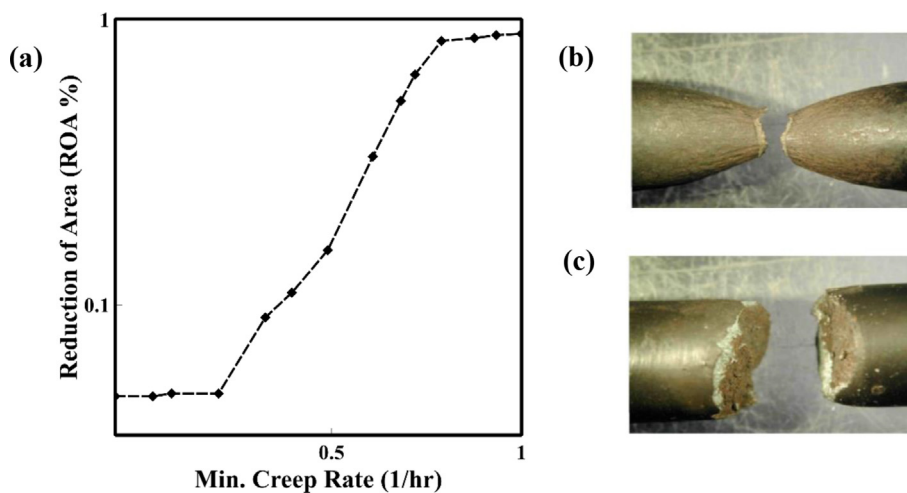


Fig. 9 – Experimental creep rupture data and fractured specimen showing stress dependency of creep ductility: a) Variation of creep ductility against the normalised stress (i.e. ratio of applied stress to yield strength) for 316H steel at 700 °C [70], b) Ductile fracture of Grade 91 plain bar tested at high stress at 550 °C (rupture time of 100 h), and c) Brittle fracture of Grade 91 plain bar tested at low stress at 650 °C (rupture time of 20,014 h) [86].

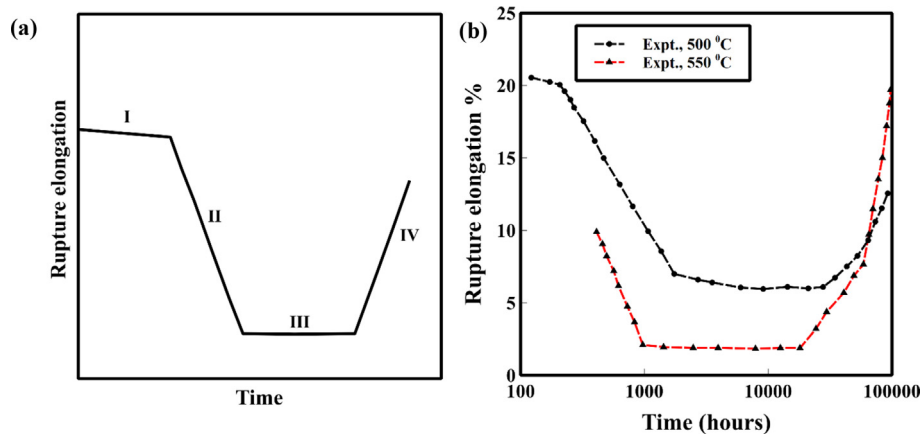


Fig. 10 – (a) A schematic diagram showing the effect of rupture time on creep rupture ductility [32], and (b) Creep rupture data for X19CrMoVNb11 steel at 500 °C and 550 °C showing the time dependent process of creep ductility in terms of rupture elongation % (Adapted from Ref [32]).

the reduction in rupture ductility is followed by a remarkable recovery in creep ductility in Regime-IV due to the ageing of microstructure in longer terms, which in turns leads to a reduction in the rate of cavity nucleation and growth and subsequent improvement in creep ductility. Experimentally, some materials were found to exhibit this variation of creep ductility with respect to time as demonstrated in Fig. 10b. The drop in creep ductility with time could be associated to the microstructural evolution and microdamage during creep exposure such as carbide coarsening [87], as shown in Fig. 11.

3.1.4. Effect of pre-straining

Since industrial powerplants operate under conditions of cycles and base loading, it becomes crucial to explore and understand the effects of pre-straining on the subsequent creep behaviour. Previous experimental and numerical studies on various steel grades have demonstrated that prior fatigue loading exhibits a paramount influence on creep properties (e.g. [88–93]). For instance, Zhang et al. [90] performed prior fatigue tests on P92 steels at 650 °C at various lifetime fractions of prior low cycle fatigue (LCF) followed by creep tests under a net section stress of 130 MPa. The study has revealed that creep ductility (in terms of creep rupture

strain) tends to gradually decrease with the percentage of lifetime fraction of prior LCF, Fig. 12a, and consequently creep life is significantly affected as presented in Fig. 12b. Similar findings were obtained by Sarkar et al. [91] for reduced activation ferritic-martensitic (RAFM) steels at 550 °C. Further, the effects of cyclic preloading on the subsequent viscoplastic deformation of austenitic stainless steel were investigated by Mayama et al. [92] and the reduction in creep rupture strain with cyclic preloading was distinctly observed.

From microstructural perspectives, the pre-straining is found to affect the local microstructure and may also promote several micro-damage mechanisms such as early recovery of the lath martensite, as shown in Fig. 13a-d, accompanied by reductions in the dislocation density [89–91,94,95], as shown in Fig. 14a-d. In the subsequent creep deformation, the early recovery of the lath martensite can transport defects to the lath boundaries, aiding in the development of creep cavities [89,90]. The degradation mechanisms resulting from pre-straining consequently lead to the deterioration of mechanical properties such as creep strength and creep ductility of the material. One criticism that may be levelled against these tests is that the high levels of plastic strain used in laboratory tests are not representative of service behaviour and thus the

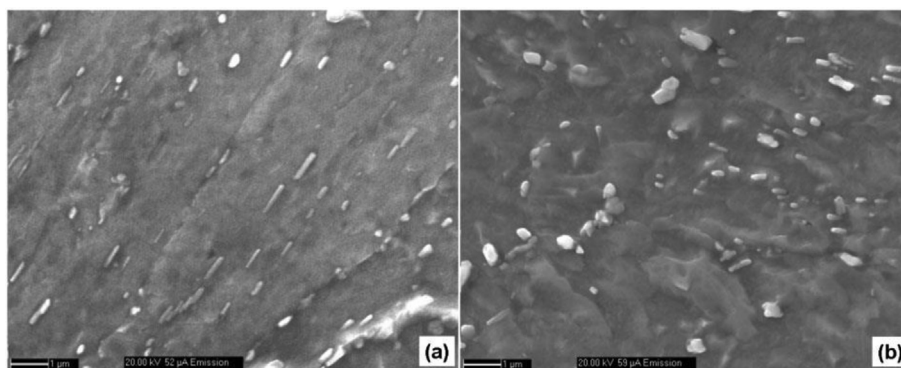


Fig. 11 – SEM images showing precipitates in 2.25Cr–1Mo steel (a) before creep testing, and (b) after creep testing (under 90 MPa net section stress and temperature 873 K) [87].

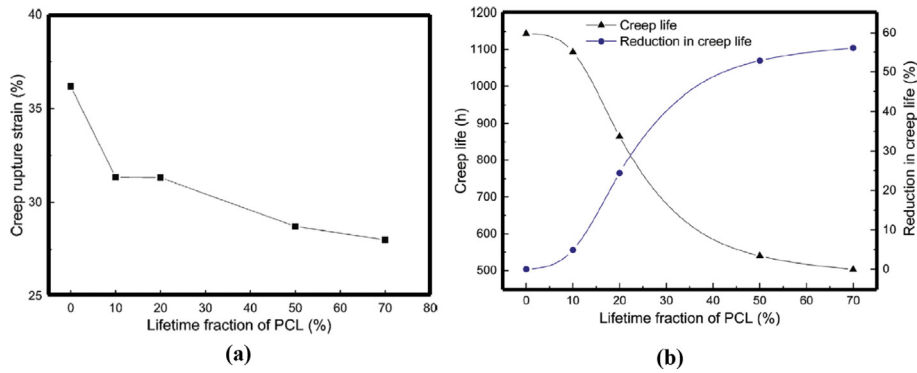


Fig. 12 – a) Variation of creep ductility with lifetime fraction of prior cyclic loading (PCL), and b) Effects of prior cyclic loading (PCL) on creep rupture life [90].

weakening effects may not necessarily capture the true creep-fatigue interaction behaviour.

3.2. Metallurgical constraints

There are some metallurgical risk factors for CSEF steels which affect creep ductility and increase steel damage susceptibility. In general, these factors are related to the chemical composition, the content of impurity/tramp elements (e.g., As, Cu, Sb, Sn), heat treatment conditions, inclusions size, distribution and content. It is crucial to

explore the influence of these factors on creep ductility to improve the creep performance of components and therefore avoid the risk of catastrophic brittle failure due to the low damage tolerance (creep ductility). The key microstructural and metallurgical factors influencing creep ductility in CSEF steels are briefly reviewed in the following sections.

3.2.1. Effects of composition and microstructure

3.2.1.1. Impurity elements. There are specific elements introduced into steel alloys during steel making and processing

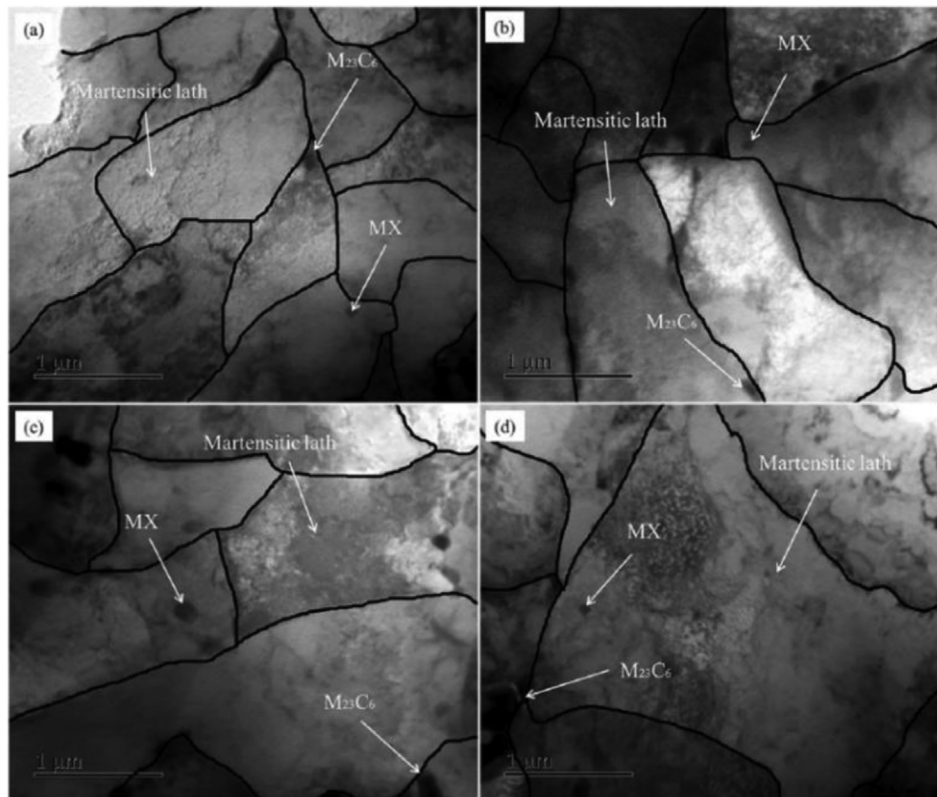


Fig. 13 – TEM images showing creep fracture for specimens with different lifetime fractions of prior LCF at (a) 0%, (b) 10%, (c) 20%, and (d) 50% [90].

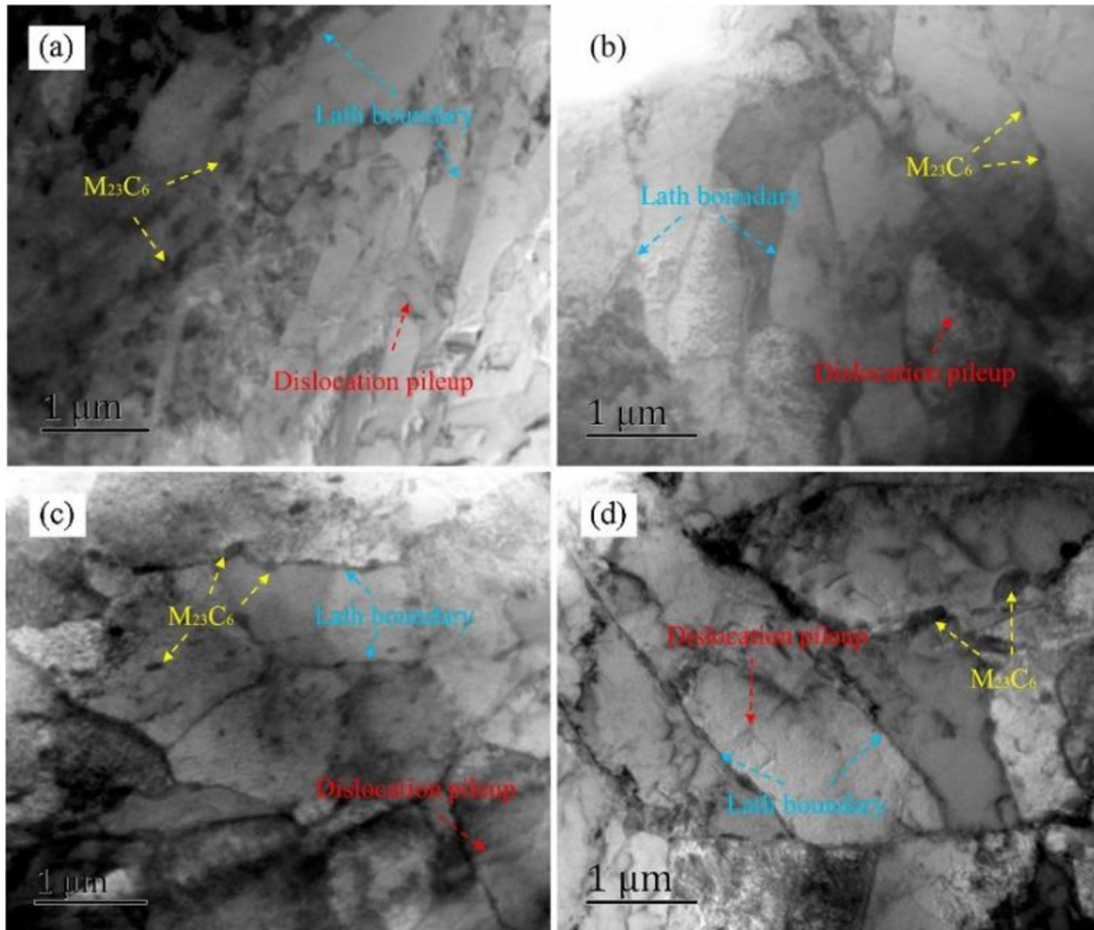


Fig. 14 – TEM images of specimens at various prior fatigue loadings: (a) as-received, (b) 20% lifetime fraction of 0.4% prior LCF, (c) 50% lifetime fraction of 0.4% prior LCF, and (d) 20% lifetime fraction of 180 s prior C–F [89].

such as Sb, Sn and Cu, which have a drastic influence on creep ductility and therefore need to be strictly controlled [27]. The presence of these elements in steel even at relatively low percentages by weight tends to reduce the boundary cohesion,

creating preferential sites for the nucleation and growth of creep cavities and consequently leading to a reduction in creep ductility [96]. Sulphur (S) also exhibits a negative influence on creep ductility when present in specific quantities as

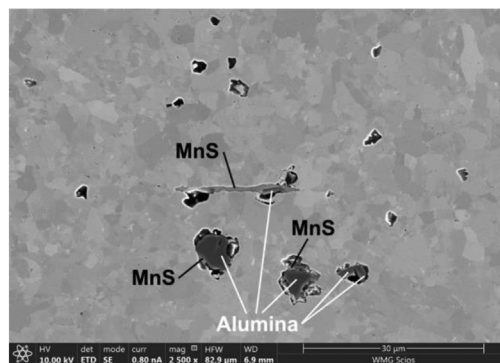
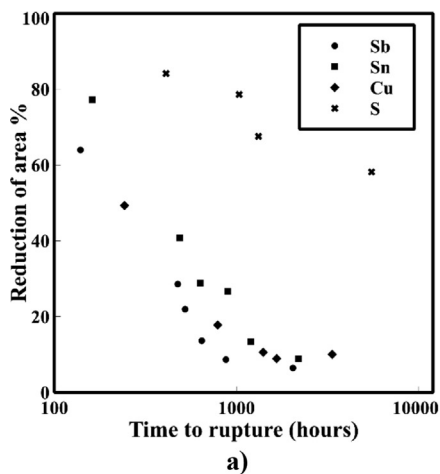


Fig. 15 – a) Effects of impurity elements (Sn, Sb, Cu and S) on creep ductility parameter reduction of area (%) for Grade 91 steel at 650 °C (Experimental data are adapted from ref [96]), and b) Association of creep damage with an inclusion cluster (MnS and Al₂O₃) in Grade 91 steel creep tested at 625 °C and 60 MPa [26].

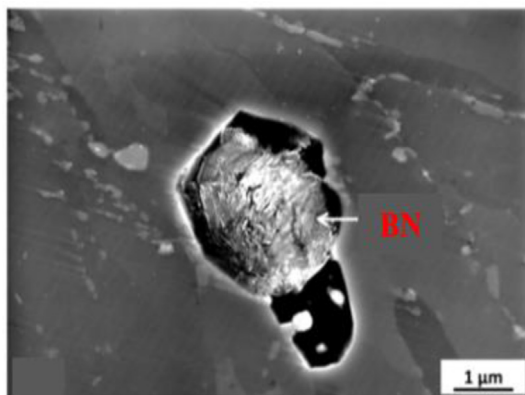


Fig. 16 – Micrograph image showing the development of creep cavities associated with BN particles in Grade 92 CSEF steel (Adapted from ref [98]).

demonstrated by previous metallurgical investigations (e.g. [26,29,84]). It was suggested that the presence of this element in sufficient quantities would lead to the formation of a large number density of inclusions such as MnS, which act as initiation sites for creep cavities, as illustrated in Fig. 15b, reducing the creep ductility and lowering the creep life [26,29]. Further, the presence of Sulphur precipitates was found to weaken the interface between matrix and particles (decohesion), leading to increased cavitation and significant reductions in creep ductility [84]. The effects of the impurity elements on creep ductility (in terms of reduction of area %) of Grade 91 steel at 650 °C are illustrated in Fig. 15a, which shows a remarkable reduction in creep ductility for heats incorporating high levels of impurity elements.

3.2.1.2. *Content of boron.* Boron (B) is used as an alloying addition in CSEF steels and under specific heat treatment conditions to improve the creep performance of these steels [27]. However, it has been observed that when excessive levels of Boron are used, this will increase the risk of forming BN inclusions, Fig. 16, which have negative impacts on creep

ductility as these inclusions could act as initiation sites for creep cavities and therefore reducing creep ductility and creep rupture life [27,37,38,97,98]. Further, like AlN inclusions, the formation of BN inclusions can also reduce the amount of Nitrogen available in the matrix and limit the formation of MX carbides, which are required to maintain good strength at high-temperature conditions [25,26].

3.2.2. *Effect of material heterogeneity (weld microstructure)* Localised creep damage and failure of welded joints present a major concern for the structural integrity of high-temperature components. The susceptibility of the weldment region to creep damage has been linked with additional variables pertinent to the weld microstructure which can influence creep ductility of welded components and increase the risk of brittle failure. One of these factors is the non-homogenous microstructure of the heat-affected zone (HAZ) in CSEF steel, which can be subdivided into three microstructural regions: the completely transformed zone (CTZ), partially transformed zone (PTZ) and over tempered zone (OTZ), as shown schematically in Fig. 17 [97–99]. Among the different HAZ regions, the partially transformed zone shows incomplete dissolutions of the pre-existing precipitates during welding and inhomogeneous distributions of the $M_{23}C_6$ carbides on lath and grain boundaries [33,98], resulting in less restraining to the grain boundary sliding and increased cavitation density [33,34,99]. Other microstructural features in CSEF weldment which influence creep ductility and promote the formation and/or growth of cavities involve the presence of secondary phase particles (e.g., Al_2O_3 and BN phases) above a critical size, which normally act as potential sites for cavity formation [26,98]. These inclusions are not dissolved in the partial dissolution zone as they will only dissolve at higher temperatures.

4. Existing creep ductility-based constitutive models

In this section, the state-of-the-art creep ductility-based constitutive models are reviewed. Analytical models representing creep ductility under uniaxial stress state are

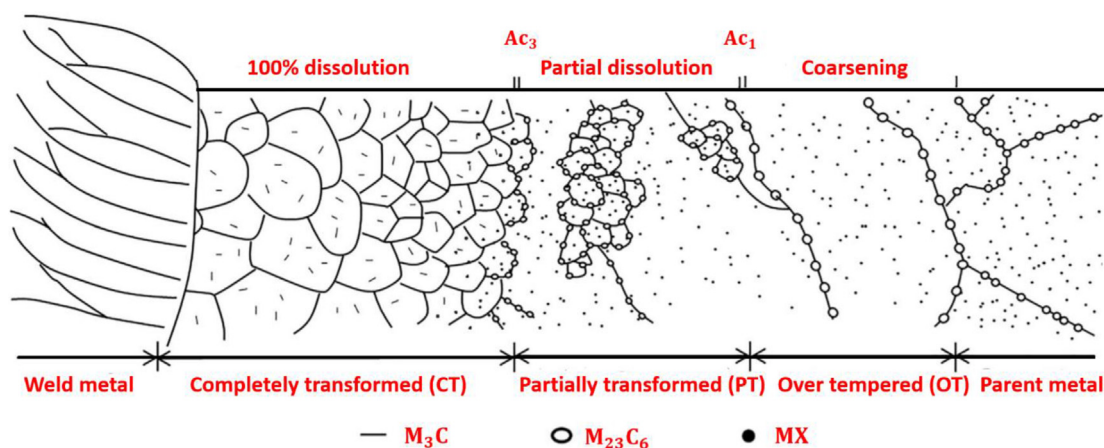


Fig. 17 – A schematic showing the classification of the HAZ microstructure in an as-welded single-pass 9% Cr steel weldment [33,99].

introduced in Section 4.1, while those relevant to multiaxial creep ductility are investigated in Section 4.2.

4.1. Uniaxial creep ductility models

As discussed in Section 3, creep ductility under uniaxial stress state is influenced by many factors including operating conditions such as the applied stress, stress states, temperature and strain rates. The variation of creep ductility with these conditions is associated with different void growth mechanisms, plastic hole growth, diffusion-controlled cavity growth and constrained cavity growth [83]. On this context, a number of creep ductility based models have been proposed to take into account the influence of these mechanisms on the uniaxial creep ductility and to represent the three creep rupture regimes shown in Fig. 7. Some of these models are briefly reviewed and appreciated below.

4.1.1. R5-2003 assessment procedure

In the R5 assessment procedure (R5-2003), an empirical model is proposed to characterise the effect of temperature (T) and creep strain rates ($\dot{\epsilon}_c$) on the uniaxial creep ductility (ϵ_{cu}) as follows [100]:

$$\epsilon_{cu} = \min \left(\epsilon_{cu,u}, \max \left(\epsilon_{cu,l}, C_0 \exp \left(\frac{C_1}{T} \right) \dot{\epsilon}_c^{C_2} \right) \right) \quad (9)$$

With reference to Equation (9) and Fig. 7, $\epsilon_{cu,u}$ represents uniaxial creep ductility on Regime-I (upper plateau), which can be determined from accelerated creep tests. $\epsilon_{cu,l}$ represents creep ductility on Regime-III (lower shelf), which can be measured based on long-term creep tests. The transition region (i.e., Regime-II), where ductility reduces with a decrease in creep strain rates, is represented by the exponential term. C_i ($i = 0, 1, 2$) are material constants obtained by fitting the experimental uniaxial creep rupture data with the empirical model.

4.1.2. Stress modified ductility approach

The model adopted in the R5-2003 assessment procedure, Equation (9), has been shown to give conservative predictions of creep damage at low-stress regime [70]. Therefore, to avoid these limitations and improve the prediction capability of the model, a modified ductility model has been proposed by Spindler [101,102], which considers the effect of stress level on creep ductility as given below:

$$\epsilon_{cu} = \min \left(\epsilon_{cu,u}, \max \left(\epsilon_{cu,l}, C_0 \exp \left(\frac{C_1}{T} \right) \dot{\epsilon}_{min}^{C_2} \sigma^{C_3} \right) \right) \quad (10)$$

where σ and $\dot{\epsilon}_{min}$ are the applied stress and minimum creep rate, respectively. The other symbols are as defined earlier. The modified model, as given by Equation (10), has been included in the R5-2014 assessment procedure and has shown more accurate creep damage predictions as opposed to the former version (R5-2003) [70].

4.1.3. Evans-wilshire model

Evans and Wilshire [103] proposed an empirical relation, Equation (11), to quantify the effect of stress and temperature variations on creep ductility under uniaxial stress state. In this

model, the transition region (Regime-II) is represented by an exponential parametric function of the applied stress and temperature as expressed below:

$$\epsilon_{cu} = \min(\epsilon_{cu,u}, \max(\epsilon_{cu,l}, \exp(C_0 + C_1\sigma + C_2T + C_3\sigma T))) \quad (11)$$

where the constants C_i ($i = 0, 1, 2, 3$) are obtained by fitting the experimental creep rupture data with Equation (11).

4.1.4. Uniaxial ductility model coupled with material pedigree function

The empirical models introduced above, Equations 9–11, characterise creep ductility in terms of the strain rates, temperature and stress levels. As discussed in Section 3, creep ductility is also dependent on chemical composition, which may exhibit a paramount influence. For low alloy steels such as CrMoV steel, creep ductility is also influenced by the prior austenite grain size. To capture the effects of these metallurgical factors on creep ductility, Binda et al. [84] proposed an empirical model with material pedigree function for 1CrMoV steel based on Spindler's stress modified ductility model as given below:

$$\epsilon_{cu} = \min \left(\epsilon_{cu,u}, \max \left(\epsilon_{cu,l}, C_0 \exp \left(\frac{C_1}{T} \right) \dot{\epsilon}_{min}^{C_2} \sigma^{C_3} f(MP) \right) \right) \quad (12)$$

where $f(MP)$ is a material pedigree function to quantify the effects of chemical composition and heat treatment conditions on creep ductility. The other symbols are as defined earlier. The model has shown a good capability to predict creep ductility characteristics of 1CrMoV steel at 550 °C, as shown in Fig. 18.

4.2. Multi-axial creep ductility-based models

As components are typically operating under complex multi-axial stress state conditions, predictive models considering

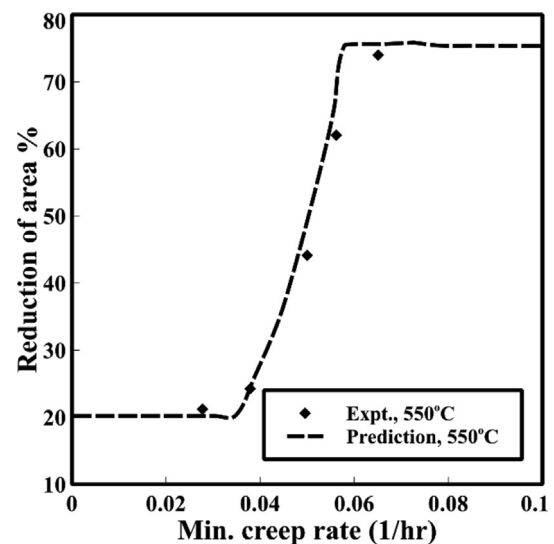


Fig. 18 – Comparison of the measured creep rupture ductility (in terms of reduction of area %) and the predicted values using Equation (12) for 1CrMoV steel at 550 °C (Adapted from ref [84]).

the effect of stress state on creep ductility are hugely important. In the literature, many models have been developed, which are generally based on the growth of a void in a deforming medium. These models relate uniaxial creep ductility to multiaxial creep ductility as a function of the stress triaxiality factor ($\frac{\sigma_m}{\sigma_e}$). Numerous multiaxial ductility-based models are reviewed in the following subsections. Physically based models are reviewed in Section 4.2.1, while the empirical or semi-empirical models are reviewed in Section 4.2.2.

4.2.1. Physically based multiaxial ductility models

4.2.1.1. Rice-Tracey model. Rice and Tracey [63] developed a physically based model, which considers the effect of multiaxiality on cavity growth in elastic-perfectly plastic materials. The model expresses the multiaxial ductility factor ($\frac{\epsilon_{cu}^*}{\epsilon_{cu}}$) in term of the stress triaxiality factor ($\frac{\sigma_m}{\sigma_e}$) as given in Equation

$$\frac{\epsilon_{cu}^*}{\epsilon_{cu}} = \exp\left(\frac{1}{2} - \frac{3\sigma_m}{2\sigma_e}\right) \tag{13}$$

where ϵ_{cu}^* is the multiaxial creep ductility; σ_m and σ_e represent the hydrostatic stress and effective stress, respectively.

4.2.1.2. Cocks-Ashby model. Another physical-based model is proposed by Cocks and Ashby [64], which assumes that, under multiaxial stress states, the growth of grain boundary cavities occurs due to the power-law creep of the surrounding grains. The model is expressed as follow:

$$\frac{\epsilon_{cu}^*}{\epsilon_{cu}} = \frac{\sinh\left[\frac{2}{3}\left(\frac{n-0.5}{n+0.5}\right)\right]}{\sinh\left[2\left(\frac{n-0.5}{n+0.5}\right)\frac{\sigma_m}{\sigma_e}\right]} \tag{14}$$

where n is the stress exponent under the secondary creep.

A ductility exhaustion model is often employed with the Cocks-Ashby model, where creep damage evolution at a given material point is defined by the following:

$$\frac{d\omega}{dt} = \frac{\dot{\epsilon}_c}{\epsilon_{cu}^*} \tag{15}$$

Cocks-Ashby model has been widely adopted to compute the multi-axial creep ductility and to predict creep damage, crack growth and failure in many engineering materials under multi-axial stress states [30,49,51,104–106]. The material constants in the Cocks-Ashby model for various materials are listed in Table 2. It can be noted that testing temperatures of the stainless steel and the carbon steel are at the very lowest end on the creep range whereas that of P92 is at the upper end.

4.2.1.3. Wen and Tu model. Wen and Tu [15] developed a multiaxial ductility model based on cavity growth and coalescence at grain boundaries, assuming that the growth of cavities is only controlled by power-law creep. In this model, the viscoplastic cavity growth mechanism is considered to control the rate of cavitation growth. The model, Equation (16), has a similar form to that of Cocks and Ashby model, except that the \sinh function in Cocks-Ashby model is replaced by an exponential term in Wen-Tu model as given below, resulting in more reliable multi-axial creep ductility predictions at lower triaxiality stress state.

$$\frac{\epsilon_{cu}^*}{\epsilon_{cu}} = \frac{\exp\left[\frac{2}{3}\left(\frac{n-0.5}{n+0.5}\right)\right]}{\exp\left[2\left(\frac{n-0.5}{n+0.5}\right)\frac{\sigma_m}{\sigma_e}\right]} \tag{16}$$

Further, a multi-axial creep constitutive model was proposed based on modified cavity growth and microcrack interaction theories [15] and given by:

$$\dot{\epsilon}_{ij}^c = \frac{3}{2} A \sigma_{eq}^{n-1} S_{ij} \exp\left(\frac{2(n+1)}{\pi\sqrt{1+\frac{3}{n}}}\right) t^m \tag{17}$$

where A, n, m are material constants; S_{ij} and ϵ_{ij}^c ($i, j = 1, 2, 3$) are the deviatoric stress tensor and creep strain tensor, respectively. The damage evolution is typically defined as given by Equation (15).

Wen-Tu ductility-based damage model was applied to simulate creep damage and crack growth behaviour in different engineering materials [107–110] and was generally found to yield more consistent results of cavity growth rates and multi-axial creep ductility compared with Cocks-Ashby model [15].

To account for the effects of creep damage and stress state on creep deformation, an improved multi-axial creep constitutive model was proposed by Wen et al. [44] and implemented to simulate creep crack growth in C-Shaped Tension and Compact Tension (CT) specimens of 316H steel tested at 550 °C. In their model [44], creep deformation and damage are coupled as expressed in the below equations:

$$\dot{\epsilon}_{ij}^c = \frac{3}{2} B \sigma_{eq}^{n-1} S_{ij} \left[1 + \beta \left(\frac{\sigma_1}{\sigma_{eq}}\right)^2\right]^{\frac{n+1}{2}} \tag{18}$$

where B, n are material constants; σ_1 is the maximum principal stress.

β is a stress independent function reflecting material behaviour and expressed by the following:

$$\beta = \frac{2\rho}{n+1} + \frac{(2n+3)\rho^2}{n(n+1)^2} + \frac{(n+3)\rho^3}{9n(n+1)^3} + \frac{(n+3)\rho^4}{108n(n+1)^4} \tag{19a}$$

Table 2 – Material parameters in Cocks-Ashby model for different materials.

Material	Temperature (° C)	Creep exponent (n)	Uniaxial creep ductility (ϵ_{cu}) %
316H stainless steel [51]	550	10.62	21
Carbon–manganese steel [104]	360	10.0	18
ASME P92 steel [105]	650	5.23	16
316H steel [49]	550	10.18 (average)	7.1 (average)

Table 3 – Material parameters in Wen-Tu model for different materials.

Material	Temperature (°C)	A	n	m	Uniaxial creep ductility (ϵ_{cu}) %
316H stainless steel [15]	550	2×10^{-19}	6.0	-0.434	8
P92 steel [108]	650	1.3×10^{-23}	4.36	-0.43	12
T91 steel [107]	550	5.87×10^{-36}	13.2	-	28.3

The parameter ρ characterises the microcrack damage and primarily depends on the number of micro-cracks per unit volume and their average diameter [44] and given as follow:

$$\rho = \frac{2(n + 1)}{\pi(1 + \frac{3}{n})^{1/3}\omega^{3/2}} \tag{19b}$$

Table 3 below shows the material parameters of Wen-Tu damage model for selected materials.

4.2.1.4. Multiaxial ductility-based model involving void shape change. In the original void growth model proposed by Cocks and Ashby [64], void is assumed to remain spherical in shape during creep. Although this assumption is found to be reasonable for mid stress triaxiality range ($2/3 \leq \frac{\sigma_m}{\sigma_e} < 2$), it is not applicable when stress triaxiality is significantly lower ($1/3 \leq \frac{\sigma_m}{\sigma_e} < 2/3$) [111]. To overcome this limitation, a micro-mechanism based void growth model involving void shape evolution during creep deformation is developed by Hu et al. [111] based on Cocks-Ashby model. Analytical solutions are given for the multi-axial creep life and creep ductility respectively in the following forms:

$$t_f \geq t_n + \frac{1}{\dot{\epsilon}_{min}} \left[\int_{f_i}^{f_c} \frac{(1 - f_h)^n}{(1 + D)^{n/2} - (1 - f_h)^{n+1}} df_h + \frac{2f_c}{3} * \frac{(1 - f_c)^n}{(1 + D_c)^{n/2} - (1 - f_c)^{n+1}} \ln \beta_{c,m} \right] \tag{20}$$

$$\epsilon_{cu}^* \leq \dot{\epsilon}_{min} t_f + \frac{4\beta_{c,m} l}{3d_g} \left[\left(2 - \frac{1}{\beta_{c,m}} \right) \sqrt{f_c^3} - \sqrt{f_i^3} \right] \tag{21}$$

where t_n and t_f are time at void nucleation and creep lifetime, respectively; ϵ_{cu}^* is the multiaxial creep ductility; $\dot{\epsilon}_{min}$ is the steady state creep strain rate; f_h is void area fraction; f_i and f_c are void area fractions at nucleation and coalescence, respectively; $\beta_{c,m}$ is void aspect ratio at failure under multi-axial stress state. l is the radius of isolate cylinder and d_g is the grain size. The terms D and D_c in the multiaxial creep lifetime expression are related to the stress triaxiality ratio μ through the following equations:

$$D = 3 \left[\frac{(1 - f_h)(\mu - 1/3)^2}{\ln f_h} \right] \tag{22.a}$$

At coalescence, D_c is given by:

$$D_c = 3 \left[\frac{(1 - f_c)(\mu - 1/3)^2}{\ln f_c} \right] \tag{22.b}$$

The model showed good agreements with the multi-axial creep rupture data and improved predictions of creep life and multiaxial creep ductility. Further, it was shown that creep

rupture life and creep ductility are significantly affected by the void shape changes in the range of low stress triaxiality [111].

4.2.2. Empirical and semi-empirical models

4.2.2.1. Manjoine models. Manjoine [112] studied the effects of stress state on creep ductility of Type 304 steel at 593 °C and proposed an empirical model where creep ductility is inversely proportional to the stress triaxiality factor as follows:

$$\frac{\epsilon_{cu}^*}{\epsilon_{cu}} = \frac{\sigma_e}{3 \sigma_m} \tag{23}$$

In later work by Manjoine [113], another empirical relation was developed following a series of notched bar tests on a range of materials to better characterise the multiaxial creep ductility and creep fracture behaviour characteristics. The proposed relation is given below:

$$\frac{\epsilon_{cu}^*}{\epsilon_{cu}} = 2 \left(1 - \frac{\sigma_m}{3\sigma_e} \right) \tag{24}$$

4.2.2.2. Spindler multiaxial ductility model. The multiaxial ductility models introduced earlier account only for the effect of stress multiaxiality on cavitation growth without any consideration to the effect of cavity nucleation on creep ductility. To overcome this shortcoming, Spindler [114] developed a semi-empirical ductility model based on the model developed by Rice and Tracey [63], Equation (13). The model comprises two terms to capture the effects of multi-axiality on both cavity nucleation and growth. The cavity nucleation term is assumed to depend on the maximum principal stress component while the cavity growth term is defined in terms of the stress triaxiality as illustrated below:

$$\frac{\epsilon_{cu}^*}{\epsilon_{cu}} = \exp \left[p \left(1 - \frac{\sigma_1}{\sigma_e} \right) + q \left(\frac{1}{2} - \frac{3\sigma_m}{2\sigma_e} \right) \right] \tag{25}$$

where p and q are material constants obtained from fitting Equation (25) with experimental multi-axial creep rupture data. The typical values of these constants for a range of materials are listed in Table 4. It can be noted that Spindler model can be reduced to that proposed by Rice and Tracey when $p = 0$ and $q = 1$, and it is also identical to that of Manjoine [113] (Equation (24)) when $p = 0$ and $q = 2\ln(2)$.

Table 4 – Material constants in Spindler ductility model for different materials.

Material	Temperature (°C)	p	q
Type 304 stainless steel [114]	593	2.38	1.04
Type 316 stainless steel [114]	593	0.15	1.25
Nickel based superalloy [115]	750	0.15	1.25
CrMoV steel [116]	575	1.5	1.2

4.2.2.3. *Modified Wen-Tu model.* In order to avoid an over conservative estimation of the multi-axial creep ductility when the stress triaxiality ratio is very large, a modified ductility-based model was proposed by Zhang et al. [117] based on Wen-Tu creep damage model and implemented to simulate creep damage and crack growth behaviour of 9Cr–1Mo steel at 600 °C [109,117]. In their work, the relationship between multi-axial and uniaxial creep ductility is defined as follow:

$$\frac{\epsilon_{cu}^*}{\epsilon_{cu}} = a * \frac{\exp\left[\frac{2}{3} \left(\frac{n-0.5}{n+0.5}\right)\right]}{\exp\left[2 \left(\frac{n-0.5}{n+0.5}\right) \frac{\sigma_m}{\sigma_e}\right]} + b \quad (26)$$

where *a* and *b* are material constants, with typical values of 0.9574 and 0.0426, respectively for 9Cr–1Mo steel [117]. This indicates that the modified model maintains a constant multi-axial ductility when the stress triaxiality ratio is very large, as shown in Fig. 19.

4.2.2.4. *Multi-scale ductility constraint model.* Nikbin [45] proposed a multi-scale ductility constraint model to predict creep rupture and crack growth under uniaxial and multi-axial stress states. The model links the global constraint (due to geometry) with microstructural constraint (from creep diffusion) at sub-grain level. In this approach, creep ductility is defined in terms of Monkman-Grant ductility rather than creep rupture strain [45], and therefore the accumulation of creep damage at any time is given by:

$$\omega = \int_0^{t_f} \frac{\dot{\epsilon}_c}{\epsilon_{MG}^*} dt \quad (27)$$

where ϵ_{MG}^* is the multi-axial Monkman Grant ductility, which can be obtained from void growth models.

In addition, Yatomi and Nikbin [118] presented a semi-empirical model based on Cocks–Ashby model by noting that the value of stress exponent (*n*) lies between 5 and 15 for

most engineering materials [118], and therefore Cocks-Ashby model can be further simplified into the following form:

$$\frac{\epsilon_{cu}^*}{\epsilon_{cu}} = \frac{0.61}{\sinh\left[\sqrt{3} \frac{\sigma_m}{\sigma_e}\right]} \quad (28)$$

5. Appraisal of the existing models and recommendations

In this section, we offer a comprehensive appraisal of the existing creep ductility-based models reviewed in the previous section. The capabilities and advantages of several commonly used multi-axial creep ductility-based models are discussed in Section 5.1, while the associated major limitations and challenges are elucidated in Section 5.2. Finally, the fundamental requirements for future improvement are recommended in Section 5.3.

5.1. Capabilities and advantages of the existing models

The existing multi-axial creep ductility-based models offer numerous capabilities and hold several key advantages.

5.1.1. Capability to predict multi-axial creep ductility

Multi-axial creep ductility-based models can reasonably predict the reduction in creep ductility under multi-axial stress states, in satisfactory agreement with the experimental observations [76,77,82]. Further, they can provide a very good approximation of the multi-axial creep ductility for a range of stress triaxiality ratios, as illustrated in Fig. 20.

5.1.2. Capability to predict multi-axial creep damage and creep rupture life

In many situations, multi-axial creep ductility-based damage models have been implemented successfully to predict creep damage, creep crack growth and creep rupture life of high-

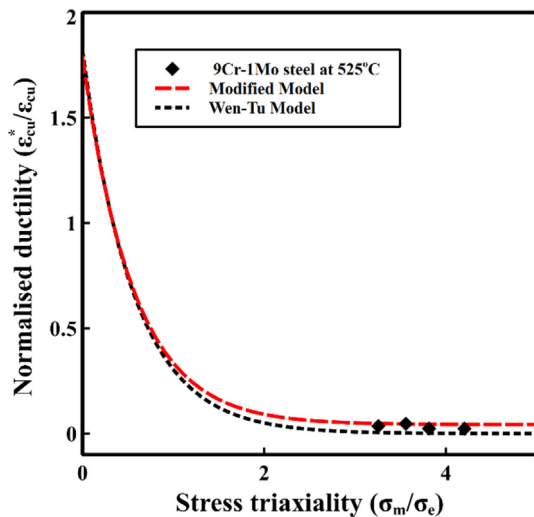


Fig. 19 – Comparison of multi-axial creep ductility predictions obtained by the modified model proposed by Zhang et al. and Wen-Tu model with the experimental data of 9Cr–1Mo steel at 525 °C (Adapted from ref [117]).

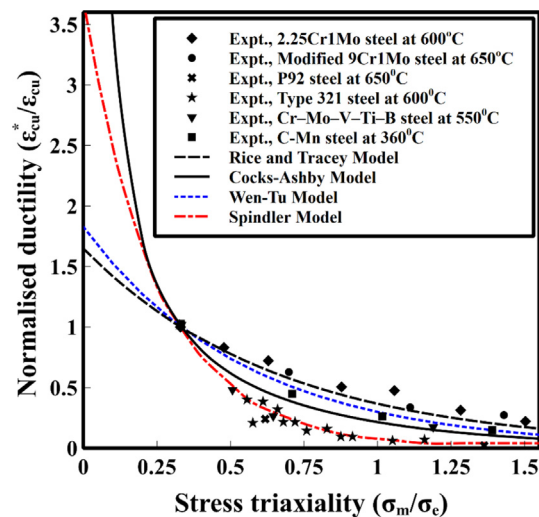


Fig. 20 – Comparison of creep ductility predicted by several multi-axial creep ductility models with the experimental data from uniaxial and multi-axial creep tests (experimental data are adapted from ref [70]).

temperature components with reasonable accuracy [116,117]. For instance, Wen and Tu [15] performed FE creep damage analysis using damage mechanics-based material models coupled with multi-axial creep ductility models based on power-law creep-controlled cavity growth theory to investigate the influence of creep ductility on the creep deformation and crack growth rates in C-Shaped Tension and Compact Tension specimens of 316H steel tested at 550 °C. Similar investigations have been conducted to predict creep damage and creep crack growth behaviour in 9Cr–1Mo steel [117] and 316 stainless steel at 600 °C [44,107] using creep damage models in conjunction with multi-axial ductility-based models, embedded in a FE solver. In the aforementioned studies, creep damage distribution and crack growth behaviour obtained by multi-axial creep ductility-based damage models had shown good agreement with the corresponding experimental data. In addition, creep ductility-based models have also shown excellent capabilities to predict creep damage, failure locations and cracking in welded high-temperature structures under complex multi-axial stress state conditions with a good agreement with the experimental observations [43].

5.1.3. Advantages and merits over stress-based CDM models

It is generally believed that ductility-based models can offer more accurate results than stress-based models e.g., Kachanov type model, provided appropriate knowledge of creep strain is available. In this regard, Song et al. [108] performed numerical analysis to investigate creep damage behaviour of small punch creep tests by employing different creep damage constitutive models. In their work, the ductility exhaustion model was found to yield more robust predictions concerning creep crack growth behaviour, failure position and creep rupture life than the stress-based models [108]. Another key advantage offered by creep ductility-based models is that they require relatively fewer material constants compared with the stress-based CDM models, which in turn promotes their wider applicability for creep damage and creep life assessments. Creep ductility-based models also enable the prediction of creep damage and crack growth rates for materials with different levels of creep ductility [43,119], which may not be the case with the stress-based models.

5.2. Challenges and limitations of the existing models

Despite of the advantages and capabilities given in the previous section, the existing creep ductility-based models still have some limitations, which need to be addressed as well. These are outlined in the following subsections.

5.2.1. Consideration of metallurgical risk factors in CSEF steels

The existing creep ductility-based models reviewed in this work were not developed specifically to suit the characteristics of CSEF steels and their microstructural features. As discussed in Section 3, there are a set of metallurgical risk factors linked to the microstructure of 9–12% Cr steels, which affect their creep damage susceptibility. Such critical factors are, however, disregarded by the current creep ductility-based models, which in turn limit their applicability for the CSEF steels. Although there have been some attempts to model the

effects of material microstructure and metallurgy on creep ductility through material pedigree function [84], such approaches are statistically based and may not offer a complete physical understanding of the effects of metallurgical variables on creep ductility and creep damage.

5.2.2. Representation of damage mechanisms

Most creep ductility damage models incorporate a single damage variable to represent, in many cases, material damage due to cavitation, which does not necessarily reflect the whole fracture and damage mechanisms experienced by CSEF steels. It is expected that, as the temperature and stress level change, more than a single damage mechanism may operate [21].

5.2.3. Long-term embrittlement behaviour

An accurate estimation of the long-term creep ductility (long-term embrittlement) constitutes another challenge for many creep ductility-based models. It has been experimentally observed that some CSEF steel grades exhibit a reduction in creep ductility at longer terms [22,37,87] due to possible voids coalescence and micro-cracks formation, as shown in Fig. 21. Nevertheless, creep ductility is often calculated based on the average ductility values at different stress levels [15,50,109,117], which is a compromise and therefore not very accurate. It is expected that there is a mechanism change that governs the transition from high ductility to lower ductility at longer terms.

5.2.4. Stress state representation

It is generally believed that at lower degrees of multi-axial stress states, the lode parameter has a paramount effect on critical failure strain and void coalescence [70,120]. Review of the current models has shown that the multi-axial stress state is mainly defined through the stress triaxiality ratio ($\frac{\sigma_m}{\sigma_e}$) while

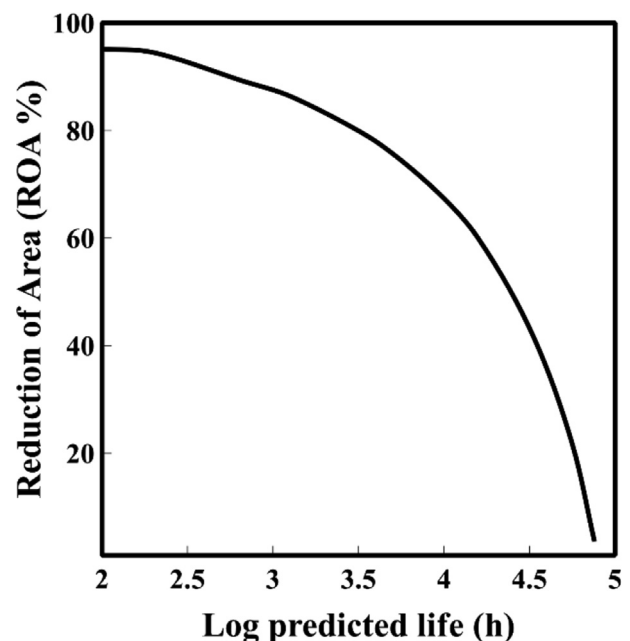


Fig. 21 – Variation of creep ductility as measured by reduction of area over creep life for Grade 92 steel at 650 °C (adapted from ref [22]).

the effect of lode parameter on creep ductility is not considered. Another limitation of some multi-axial creep ductility-based models, e.g., Cocks-Ashby model, is manifested by the infinite values predicted for creep ductility at low-stress triaxiality ratio, as shown in Fig. 21, which is not realistic and should not be used for creep life assessments. Previous investigations also pointed out that (under bi-axial loading conditions, with biaxiality ratio less than zero) the Cocks-Ashby model may give rise to non-conservative predictions [15,44]. In some situations, ductility exhaustion models have shown very limited capability to predict creep damage and creep rupture lives under bi-axial loading conditions, with more than 30% estimated error in creep life predictions [117], which emphasises the need for more robust models with a better representation of multi-axial stress states.

5.2.5. Consideration of cavity nucleation effects on creep ductility and damage

Needless to say, numerous multi-axial ductility-based models disregard the effect of cavity nucleation on creep ductility because the driving mechanisms by which cavities nucleate are not fully understood [70]. Although in the Spindler model, Equation (25), an additional term is added to quantify the effects of cavity nucleation on the multi-axial creep ductility, the model was derived based on fitting creep ductility experimental data of austenitic stainless steel and hence may not necessarily represent creep ductility characteristics of the CSEF steels.

5.2.6. Practical challenges

In this section, we will address some of the practical challenges associated with the implementation of ductility-based models for real-life applications. These are summarised below:

1. The complexity to accurately define the stress state in an operating component.
2. The complexity and uncertainty to obtain the active mechanical loads on a complex system.
3. Availability of material properties relevant to the material and age in service. For instance, how to reliably determine long-term creep properties.

Such concerns emphasise the need for relatively easy to deploy predictive models without compromising the model accuracy and the technical details.

5.3. Recommendations for future improvements

Developing improved creep ductility-based damage models for the CSEF steels is challenging yet a necessary step towards a more robust approach, which takes into account the range of relevant stress and temperature combinations and metallurgical risk factors. In view of the main limitations and challenges presented in the previous section, it is evident that future improvements need to consider several aspects to overcome these deficiencies:

1. The microstructure–property relationship should be at the heart of developing future ductility-based models to appreciate the complex metallurgy of the CSEF steels. This

necessitates the incorporation of additional state variables with a clear physical insight and linked to material microstructure and thus enable the effects of the key metallurgical constraints to be captured by the models.

2. Future improvements also need to clearly define the transition behaviour in creep ductility in a wide range of stresses and temperatures to eliminate any uncertainties with regards to the creep fracture behaviour of the CSEF steels and to predict more accurately the long-term embrittlement observed in some CSEF steel grades.
3. Future models are also required to consider more robustly the wide variability of the multi-axial creep behaviour. For this purpose, stress state representation should rely not only on one factor, e.g., the stress triaxiality ratio but also on other parameters such as the lode parameter (which is a function of the third invariant of the stress deviator and thought to control the void shape), particularly at lower triaxiality ranges.
4. It has been shown that the creep performance of the CSEF steel weldments is largely affected by the creep ductility of the base metal [97,98]. As such, future models should offer the capability to predict creep damage susceptibility of the CSEF steel weldments (BM, WM, HAZ) and to evaluate the micro-damage, cavity rate and distribution for a specific alloy composition under given stress and temperature.
5. Since creep ductility is related to creep cavitation, an improved physical understanding of the mechanisms associated with cavity nucleation and evolution utilizing advanced tools such as X-ray synchrotron tomography is crucial to developing improved ductility based constitutive models.

6. Summary

Creep ductility has important implications in high-temperature material performance and structural integrity assessment. In the present study, creep ductility definition, experimental methods, dependency, and some constitutive material models are reviewed. An appraisal of the state-of-the-art ductility-based damage models is presented, where the capabilities of the existing models are appreciated and critically examined. On this basis, the major limitations of the current models are identified and the requirements for future improvement are addressed.

Undoubtedly, proper characterization/measurement of the multi-axial creep ductility plays an important role in accurate creep damage and creep rupture lives prediction. Thus, the popular multi-axial notched bars creep ductility tests should be reappraised and improved in future work. Of particular relevance to notched bars design is the degree of multi-axiality, level of plastic strain, the extent of creep deformation and local fracture behaviour which govern the nature of multi-axial stress states and geometry-induced mechanical constraints. These aspects require further investigations through theoretical study, experiment testing and numerical modelling. Additionally, much more

emphasis should be placed on understanding the link between creep damage susceptibility and the metallurgical and mechanical constraints in CSEF steels in order to develop improved physically-based constitutive models, optimise alloy composition and design components of better performance.

Declaration of Competing Interest

The authors declare that they have no known competing financial interests or personal relationships that could have appeared to influence the work reported in this paper.

Acknowledgments

This work was supported by the Engineering and Physical Sciences Research Council (EPSRC). The funding is provided through the EPSRC Centre for Doctoral Training in Resilient Decarbonised Fuel Energy Systems (Grant number: EP/S022996/1). The work was also partly sponsored by the Net Zero Research.

REFERENCES

- [1] Masuyama F. New developments in steels for power generation boilers. In: *Advanced heat resistant steel for power generation*. Institute of Materials; 1998. p. 33–48.
- [2] Choudhary BK, Palaparti DPR. Comparative tensile flow and work hardening behaviour of thin section and forged thick section 9Cr-1Mo ferritic steel in the framework of Voce equation and Kocks-Mecking approach. *J Nucl Mater* 2012;430:72–81. <https://doi.org/10.1016/j.jnucmat.2012.06.046>.
- [3] Abe F. Precipitate design for creep strengthening of 9% Cr tempered martensitic steel for ultra-supercritical power plants. *Sci Technol Adv Mater* 2008;9(1):13002. <https://doi.org/10.1088/1468-6996/9/1/013002>.
- [4] Maruyama K, Sawada K, Koike J. Strengthening mechanisms of creep resistant tempered martensitic steel. *ISIJ Int* 2001;41(6):641–53. <https://doi.org/10.2355/isijinternational.41.641>.
- [5] Golden BJ, Li D, Guo Y, Tiernan P, Leen SB, O'Dowd NP. Microscale deformation of a tempered martensite ferritic steel: modelling and experimental study of grain and sub-grain interactions. *J Mech Phys Solid* 2016;86:42–52. <https://doi.org/10.1016/j.jmps.2015.09.015>.
- [6] Wang C, Xuan F, Zhao P. A dislocation-based constitutive model for the cyclic response of nanolath strengthened steels. *Int J Mech Sci* 2019;155:475–87. <https://doi.org/10.1016/j.ijmecsci.2019.03.010>.
- [7] Fournier B, Dalle F, Sauzay M, Longour J, Salvi M, Caës C, et al. Comparison of various 9–12%Cr steels under fatigue and CF loadings at high temperature. *Mater Sci Eng, A* 2011;528(22–23):6934–45. <https://doi.org/10.1016/j.msea.2011.05.046>.
- [8] Pesicka J, Kuzel R, Dronhofer A, Eggeler G. The evolution of dislocation density during heat treatment and creep of tempered martensite ferritic steels. *Acta Mater* 2003;51(16):4847–62. [https://doi.org/10.1016/S1359-6454\(03\)00324-0](https://doi.org/10.1016/S1359-6454(03)00324-0).
- [9] Viswanathan R, Henry JF, Tanzosh J, Stanko G, Shingledecker J, Vitalis B, et al. U.S. program on materials technology for ultra-supercritical coal power plants. *J Mater Eng Perform* 2005;14(3):281–92. <https://doi.org/10.1361/10599490524039>.
- [10] Ragab R, Parker J, Li M, Liu T, Sun W. Modelling of a Grade 91 power plant pressurised header weldment under ultrasuper-critical creep conditions. *Int J Pres Ves Pip* 2021;192:104389. <https://doi.org/10.1016/j.ijpvp.2021.104389>.
- [11] Cano JA, Stewart CM. A continuum damage mechanics (CDM) based Wilshire model for creep deformation, damage, and rupture prediction. *Mater Sci Eng, A* 2020;799:140231. <https://doi.org/10.1016/j.msea.2020.140231>.
- [12] Meng Q, Wang Z. Creep damage models and their applications for crack growth analysis in pipes: a review. *Eng Fract Mech* 2019;205:547–76. <https://doi.org/10.1016/j.engfracmech.2015.09.055>.
- [13] Li M, Barrett RA, Scully S, Harrison NM, Leen SB, O'Donoghue PE. Cyclic plasticity of welded P91 material for simple and complex power plant connections. *Int J Fatig* 2016;87:391–404. <https://doi.org/10.1016/j.ijfatigue.2016.02.005>.
- [14] Li D, Li M, Shang D, Gupta A, Sun W. Physically-based modelling of cyclic softening and damage behaviors for a martensitic turbine rotor material at elevated temperature. *Int J Fatig* 2021;142. <https://doi.org/10.1016/j.ijfatigue.2020.105956>.
- [15] Wen JF, Tu ST. A multiaxial creep-damage model for creep crack growth considering cavity growth and microcrack interaction. *Eng Fract Mech* 2014;123:197–210. <https://doi.org/10.1016/j.engfracmech.2014.03.001>.
- [16] Hosseini E, Holdsworth SR, Mazza E. Stress regime-dependent creep constitutive model considerations in finite element continuum damage mechanics. *Int J Damage Mech* 2013;22:1186–205. <https://doi.org/10.1177/2F1056789513479810>.
- [17] Yadav SD, Sonderegger B, Stracey M, Poletti C. Modelling the creep behaviour of tempered martensitic steel based on a hybrid approach. *Mater Sci Eng, A* 2016;662:330–41. <https://doi.org/10.1016/j.msea.2016.03.071>.
- [18] Wilshire B, Scharning PJ. A new methodology for analysis of creep and creep fracture data for 9–12% chromium steels. *Int Mater Rev* 2008;53(2):91–104. <https://doi.org/10.1179/174328008X254349>.
- [19] Wilshire B, Scharning PJ. Long-term creep life prediction for a high chromium steel. *Scripta Mater* 2007;56(8):701–4. <https://doi.org/10.1016/j.scriptamat.2006.12.033>.
- [20] Xu Q, Barrans S. The development of multiaxial creep damage constitutive equations for 0.5Cr-0.5Mo-0.25 V ferritic steel at 590 °C. *JSME Int J Series: A Solid Mech Mater Eng* 2003;46(1):51–9. <https://doi.org/10.1299/jsmea.46.51>.
- [21] Dyson B. Use of CDM in materials modelling and component creep life prediction. *ASME J Pressure Vessel Technol* 2000;122:281–96. <https://doi.org/10.1115/1.556185>.
- [22] Allen D. An Investigation of the factors determining creep strength and ductility in Grade 92 steel. In: *Proc. Of fourth international ECCC conference on creep & fracture in high temperature components design & life assessment; 10-14 september 2017; 2018 [Düsseldorf, Germany]*.
- [23] Brett SJ, Oates DL, Johnston C. In-service type IV cracking on a modified 9Cr (Grade 91) header. In: *ECCC conference: creep & fracture in high temperature components - design & life assessment issues. vols. 12–14. London: IMechE; 2005. 2005.*
- [24] Parker J, Brett S. Creep performance of a Grade 91 header. *Int J Pres Ves Pip* 2013;111–112:82–8. <https://doi.org/10.1016/j.ijpvp.2013.05.003>.
- [25] Siefert JA, Parker JD, Shingledecker JP. Optimization of advanced steels for cyclic operation through an integration

- of material testing, modelling and novel component test validation. DE-FE002620. EPRI Presentation; 2016. 21 April 2016.
- [26] Siefert JA. PhD thesis. In: The influence of the parent metal condition on the cross-weld creep performance in grade 91 steel. Loughborough University; 2019. <https://doi.org/10.26174/thess.lboro.8309882.v1>.
- [27] Parker J, Siefert J. Metallurgical and stress state factors which affect the creep and fracture behavior of 9% Cr steels. *Adv Mater Sci Eng* 2018;2018. <https://doi.org/10.1155/2018/6789563>. Article ID 6789563, 15 pages.
- [28] Siefert JA, Parker JD, Thomson RC. Linking performance of parent Grade 91 steel to the cross-weld creep performance using feature type tests. In: Parker J, Shingledecker J, Siefert J, editors. *Advances in materials technology for fossil power plants, proceedings of the eight international conference (EPRI 2016)*. vol. 11. Albufeira, Algarve, Portugal; 2016. p. 530–43. 14 October 2016.
- [29] Siefert JA, Parker JD, Thomson RC. Factors contributing to heat affected zone damage in Grade 91 steel feature type cross-weld tests. In: Presented at the 4th international ECCO creep & fracture conference; 2017. Dusseldorf, Germany, 10th-14th September 2017.
- [30] Xu X, Wang GZ, Xuan FZ, Tu ST. Effects of creep ductility and notch constraint on creep fracture behavior in notched bar specimens. *Mater A T High Temp* 2016;33(2):198–207. <https://doi.org/10.1080/09603409.2016.1144498>.
- [31] Parker J. Creep ductility considerations for high energy components manufactured from creep strength enhanced steels. *Mater A T High Temp* 2017;34(2):109–20. <https://doi.org/10.1080/09603409.2016.1270720>.
- [32] Holdsworth S. Creep-ductility of high temperature steels: a review. *Metals* 2019;9(3):342. <https://doi.org/10.3390/met9030342>.
- [33] Xu X, West GD, Siefert JA, Thomson RC. The influence of thermal cycles on the microstructure of grade 92 steel. *Metall Mater Trans* 2017;48:5396–414. <https://doi.org/10.1007/s11661-017-4306-4>.
- [34] Xu X, West GD, Siefert JA, Thomson RC. Microstructural characterization of the heat affected zones in grade 92 steel welds: double-pass and multi-pass Welds. *Metall Mater Trans* 2018;49:1211–30. <https://doi.org/10.1007/s11661-017-4446-6>. 2018.
- [35] Siefert J, Parker J, Maclachlan R, Yan S, Thomson R. Assessment and quantification of damage in the grade 91 steel partially transformed zone. Loughborough University; 2019. Conference contribution, <https://hdl.handle.net/2134/12443297.v1>.
- [36] Kimura K, Sawada K, Kushima H. Creep rupture ductility of creep strength enhanced ferritic steels. *ASME Journal of Pressure Vessel Technology* 2012;134(3):31403. <https://doi.org/10.1115/1.4005876>.
- [37] Abe F. Influence of boron nitride inclusions and degradation in creep rupture strength on creep rupture ductility of Gr.122. *Mater A T High Temp* 2021. <https://doi.org/10.1080/09603409.2021.1935637>.
- [38] Abe F. Influence of chemical compositions and creep test conditions on UK R5 creep ductility parameter lambda of W-Mo-balanced 9Cr steel. *Mater A T High Temp* 2020;37(5):309–20. <https://doi.org/10.1080/09603409.2020.1789805>.
- [39] Parker JD. Factors affecting Type IV creep damage in Grade 91 steel welds. *Mater Sci Eng, A* 2013;578:430–7. <https://doi.org/10.1016/j.msea.2013.04.045>.
- [40] Kobayashi S, Sawada K, Hara T, Kushima H, Kimura K. Heat-to-Heat variation in creep rupture ductility of ASME Gr.91 steels in the long-term - investigation into recovery of microstructure and void formation. In: Proceedings of the 7th international conference on advances in materials technology for fossil power plants. Hawaii: Waikoloa; 2013.
- [41] Siefert JA, Parker JD. Evaluation of the creep cavitation behavior in Grade 91 steels. *Int J Pres Ves Pip* 2016;138:31–44. <https://doi.org/10.1016/j.ijpvp.2016.02.018>.
- [42] Panait CJ, Zielinska-Lipiec A, Koziel T, Czyska-Filemonowicz A, Gourgues-Lorenzon A, Bendick W. Evolution of dislocation density, size of subgrains and MX-type precipitates in a P91 steel during creep and during thermal ageing at 600°C for more than 100,000h. *Mater Sci Eng, A* 2010;527:4062–9. <https://doi.org/10.1016/j.msea.2010.03.010>.
- [43] Ragab R, Parker J, Li M, Liu T, Sun W. Creep crack growth modelling of Grade 91 vessel weldments using a modified ductility-based damage model. *Eur J Mech Solid* 2021;91:104424. <https://doi.org/10.1016/j.euromechsol.2021.104424>.
- [44] Wen JF, Tu ST, Gao XL, Reddy JN. Simulations of creep crack growth in 316 stainless steel using a novel creep-damage model. *Eng Fract Mech* 2013;98(1):169–84. <https://doi.org/10.1016/j.engfracmech.2012.12.014>.
- [45] Nikbin K. A unified multiscale ductility exhaustion-based approach to predict uniaxial, multiaxial creep rupture and crack growth. *Eng Fract Mech* 2017;179:240–59. <https://doi.org/10.1016/j.engfracmech.2017.04.046>.
- [46] Alang N, Nikbin K. An analytical and numerical approach to multiscale ductility constraint based model to predict uniaxial/multiaxial creep rupture and cracking rates. *Int J Mech Sci* 2018;135:342–52. <https://doi.org/10.1016/j.ijmecsci.2017.11.030>.
- [47] Shlyannikov V, Tumanov A. Creep-fracture resistance parameters determination based on stress and ductility damage models. *Fatig Fract Eng Mater Struct* 2018;41:2110–29. <https://doi.org/10.1111/ffe.12766>.
- [48] Spindler MW. An improved method for calculation of creep damage during creep-fatigue cycling. *Mater Sci Technol* 2007;23(12):1461–70. <https://doi.org/10.1179/174328407X243924>.
- [49] Oh CS, Kim NH, Kim YJ, Davies CM, Nikbin KM, Dean DW. Creep failure simulations of 316H at 550°C: Part I – a method and validation. *Eng Fract Mech* 2011;78:2966–77. <https://doi.org/10.1016/j.engfracmech.2011.08.015>.
- [50] Kim NH, Oh CS, Kim YJ, Davies CM, Nikbin KM, Dean DW. Creep failure simulations of 316H at 550°C: Part II – effects of specimen geometry and loading mode. *Eng Fract Mech* 2013;105:169–81. <https://doi.org/10.1016/j.engfracmech.2013.04.001>.
- [51] Yatomi M, Davies CM, Nikbin KM. Creep crack growth simulations in 316H stainless steel. *Eng Fract Mech* 2008;75:5140–50. <https://doi.org/10.1016/j.engfracmech.2008.08.001>.
- [52] Kumar Y, Venugopal S, Sasikala G, Albert SK, Bhaduri AK. Study of creep crack growth in a modified 9Cr–1Mo steel weld metal and heat affected zone. *Mater Sci Eng, A* 2016;655:300–9. <https://doi.org/10.1016/j.msea.2015.12.053>.
- [53] Zhang Q, Zhang J, Zhao P, Huang Y, Yang Y, Zhao Y. Microstructure of 10% Cr martensitic heat-resistant steel welded joints and type IV cracking behavior during creep rupture at 650 °C. *Mater Sci Eng, A* 2015;638:30–7. <https://doi.org/10.1016/j.msea.2015.04.062>.
- [54] Hayhurst DR. high-temperature continuum damage proc. Of EPRI workshop on state of mechanics. Knowledge on continuum damage modelling. 2018; July. p. 19–20 [Prague, Czech Republic, CD-ROM].
- [55] Kassner ME. *Fundamentals of creep in metals and alloys*. 2nd ed. Oxford, U.K.: Elsevier; 2009.

- [56] Weertman J. Theory of steady-state creep based on dislocation climb. *J Appl Phys* 1955;26:1213–7. <https://doi.org/10.1063/1.1721875>.
- [57] Kimura K, Kushima H, Booker GR. Heterogeneous changes in microstructure and degradation behaviour of 9Cr–1Mo–V–Nb steel during long term creep. *Key Eng Mater* 2000;171:483–90. <https://doi.org/10.4028/www.scientific.net/KEM.171-174.483>.
- [58] Sawada K, Kushima H, Tabuchi M, Kimura K. Microstructural degradation of Gr. 91 steel during creep under low stress. *Mater Sci Eng, A* 2011;528(16):5511–8. <https://doi.org/10.1016/j.msea.2011.03.073>.
- [59] Chen RP, Armaki HG, Maruyama K, Igarashi M. Long-term microstructural degradation and creep strength in Gr. 91 steel. *Mater Sci Eng, A* 2011;528(13):4390–4. <https://doi.org/10.1016/j.msea.2011.02.060>.
- [60] Holdsworth S. Creep ductility of 1CrMoV rotor steel. *Mater A T High Temp* 2017;34:99–108. <https://doi.org/10.1080/09603409.2016.1223908>.
- [61] Monkman FC, Grant NJ. An empirical relationship between rupture life and minimum creep rate in creep-rupture tests. *Proceedings-American Soc Testing Mater* 1956;56:593–620.
- [62] Phaniraj C, Choudhary BK, Bhanu Sankara Rao K, Baldev Raj. Relationship between time to reach Monkman-Grant ductility and rupture life. *Scripta Mater* 2003;48(9):1313–8. [https://doi.org/10.1016/S1359-6462\(03\)00021-6](https://doi.org/10.1016/S1359-6462(03)00021-6). ISSN 1359-6462.
- [63] Rice JR, Tracey DM. On the ductile enlargement of voids in triaxial stress fields. *J Mech Phys Solid* 1968;17:201–17. [https://doi.org/10.1016/0022-5096\(69\)90033-7](https://doi.org/10.1016/0022-5096(69)90033-7).
- [64] Cocks ACF, Ashby MF. Intergranular fracture during power-law creep under multiaxial stresses. *Met Sci* 1980;14(8–9):395–402. <https://doi.org/10.1179/030634580790441187>.
- [65] ASTM E139-11(2018). Standard test methods for Conducting creep, creep-rupture, and stress-rupture tests of metallic materials. West Conshohocken, PA: ASTM International; 2018. www.astm.org.
- [66] En Iso 204 BS. Metallic materials. Uniaxial creep testing in tension. Method of test, British Standards Institution; 2018.
- [67] Hyde TH, Sun W, Williams JA. The requirements for and the use of miniature test specimens to provide mechanical and creep properties of materials: a review. *Int Mater Rev* 2007;52(4):213–55. <https://doi.org/10.1179/174328007X160317>.
- [68] Morris A, Cacciapuoti B, Sun W. The role of small specimen creep testing within a life assessment framework for high temperature power plant. *Int Mater Rev* 2018;63(2):102–37. <https://doi.org/10.1080/09506608.2017.1332538>.
- [69] Webster GA, Nikbin KM, Biglari F. Finite element analysis of notched bar skeletal point stresses and dimension changes due to creep. *Fatig Fract Eng Mater Struct* 2004;27:297–303. <https://doi.org/10.1111/j.1460-2695.2004.00704.x>.
- [70] Wen JF, Tu ST, Xuan FZ, Zhang XW, Gao XL. Effects of stress level and stress state on creep ductility: evaluation of different models. *J Mater Sci Technol* 2016;32(8):695–704. <https://doi.org/10.1016/j.jmst.2016.02.014>.
- [71] Sakane M, Tokura H. Experimental study of biaxial creep damage for type 304 stainless steel. *Int J Damage Mech* 2002;11(3):247–62. <https://doi.org/10.1106/2F105678902026412>.
- [72] Hayhurst DR. Creep rupture under multi-axial states of stress. *J Mech Phys Solid* 1972;20(6):381–2. [https://doi.org/10.1016/0022-5096\(72\)90015-4](https://doi.org/10.1016/0022-5096(72)90015-4).
- [73] Rees DWA. Requirements for thin-walled torsion testing. In: Gooch DJ, How IM, editors. *Techniques for multiaxial creep testing*. Dordrecht: Springer; 1986. https://doi.org/10.1007/978-94-009-3415-3_3.
- [74] Delobelle P, Trivaudey F, Oytana C. High temperature creep damage under biaxial loading: INCO 718 and 316 (17-12 SPH) steels. *Nucl Eng Des* 1989;114:365–77. [https://doi.org/10.1016/0029-5493\(89\)90114-3](https://doi.org/10.1016/0029-5493(89)90114-3).
- [75] Cane BJ. Stress state distributions in thick-walled pressurised tubes under creep loading. In: Gooch DJ, How IM, editors. *Techniques for multiaxial creep testing*. Dordrecht: Springer; 1986. https://doi.org/10.1007/978-94-009-3415-3_15.
- [76] Goyal S, Laha K, Das CR, Panneerselvi S, Mathew MD. Effect of Constraint on creep behavior of 9Cr-1Mo steel. *Metall Mater Trans* 2014;45:619–32. <https://doi.org/10.1007/s11661-013-2025-z>.
- [77] Goyal S, Laha K. Creep life prediction of 9Cr–1Mo steel under multiaxial state of stress. *Mater Sci Eng, A* 2014;615:348–60. <https://doi.org/10.1007/s11661-013-2025-z>.
- [78] Yatomi M, Bettinson AD, O’ Dowd NP, Nikbin KM. Modelling of damage development and failure in notched-bar multiaxial creep tests. *Fatig Fract Eng Mater Struct* 2004;27:283–95. <https://doi.org/10.1111/j.1460-2695.2004.00755.x>.
- [79] Niu T, Zhao P, Zhu G, Gong J, Xuan F. Stress state dependent creep damage behavior of 9–12% Cr steel notched components. *Mater Sci Eng, A* 2021;804:140762. <https://doi.org/10.1016/j.msea.2021.140762>.
- [80] Ni Y, Xu H, Chang Y, Mao X. Research on elastic-plastic creep damage of notched P92 steel specimens. *Mater A T High Temp* 2018;35(4):335–42. <https://doi.org/10.1080/09603409.2017.1335961>.
- [81] Alang NA. Prediction of long-term static and cyclic creep rupture and crack growth of Grade 92 steel under different stress states. PhD Thesis. Imperial College London; 2018. <https://doi.org/10.25560/60640>.
- [82] Chang Y, Xu H, Ni Y, Lan X, Li H. The effect of multiaxial stress state on creep behavior and fracture mechanism of P92 steel. *Mater Sci Eng* 2015;70–6. <https://doi.org/10.1016/j.msea.2015.03.056>.
- [83] Hales R. The role of cavity growth mechanisms in determining creep-rupture under multiaxial stresses. *Fatig Fract Eng Mater Struct* 1994;17:579–91. <https://doi.org/10.1111/j.1460-2695.1994.tb00257.x>.
- [84] Binda L, Holdsworth SR, Mazza E. The exhaustion of creep ductility in 1CrMoV steel. *Int J Pres Ves Pip* 2010;87:319–25. <https://doi.org/10.1016/j.ijpvp.2010.03.019>.
- [85] Spindler MW. The multiaxial and uniaxial creep ductility of Type 304 steel as a function of stress and strain rate. *Mater A T High Temp* 2004;21(1):47–54. <https://doi.org/10.1179/mht.2004.007>.
- [86] Cipolla L, Di Gianfrancesco A, Venditti D, Cumino G, Caminada S. Microstructural evolution during long term creep tests of 9%Cr steel grades. In: *Proceedings of the ASME 2007 pressure vessels and piping conference*. vol. 9. San Antonio, Texas, USA: ASME; 2007. p. 445–59. <https://doi.org/10.1115/CREEP2007-26030>. Eighth international conference on creep and fatigue at elevated temperatures.
- [87] Goyal S, Laha K, Panneer Selvi S, Mathew MD. Mechanistic approach for prediction of creep deformation, damage and rupture life of different Cr–Mo ferritic steels. *Mater A T High Temp* 2014;31(3):211–20. <https://doi.org/10.1179/1878641314Y.0000000016>.
- [88] Erinoshio T, Venkata K, Mostafavi M, Knowles D, Truman C. Influence of prior cyclic plasticity on creep deformation using crystal plasticity modelling. *Int J Solid Struct* 2018;139:129–37. <https://doi.org/10.1016/j.jisolsolstr.2018.01.028>.

- [89] Zhang W, Wang X, Chen H, Zhang T, Gong J. Microstructural damage mechanics-based model for creep fracture of 9%Cr steel under prior fatigue loading. *Theor Appl Fract Mech* 2019;103. <https://doi.org/10.1016/j.tafmec.2019.102269>.
- [90] Zhang W, Wang X, Gong J, Jiang Y, Huang X. Experimental and simulated characterization of creep behavior of P92 steel with prior cyclic loading damage. *J Mater Sci Technol* 2017;33:1540–8. <https://doi.org/10.1016/j.jmst.2017.09.006>.
- [91] Sarkar A, Vijayanand V, Parameswaran P, Shankar V, Sandhya R, Laha K, et al. Influence of prior fatigue cycling on creep behavior of reduced activation ferritic-martensitic steel. *Metall Mater Trans* 2014;45:3023–35. <https://doi.org/10.1007/s11661-014-2237-x>.
- [92] Mayama T, Sasaki K. Investigation of subsequent viscoplastic deformation of austenitic stainless steel subjected to cyclic preloading. *Int J Plast* 2006;22(2):374–90. <https://doi.org/10.1016/j.ijplas.2005.03.008>.
- [93] Joseph T, McLennon D, Spindler M, Truman C, Smith DJ. The effect of prior cyclic loading variables on the creep behaviour of ex-service Type 316H stainless steel. *Mater A T High Temp* 2013;30(2):156–60. <https://doi.org/10.3184/096034013X13717271415898>.
- [94] Raea Y, Guo X, Benaarbia A, Neate N, Sun W. On the microstructural evolution in 12% Cr turbine steel during low cycle fatigue at elevated temperature. *Mater Sci Eng, A* 2020;773:138864. <https://doi.org/10.1016/j.msea.2019.138864>.
- [95] Zhang W, Wang X, Li X, Gong J, Abdel Wahab M. Influence of prior low cycle fatigue on microstructure evolution and subsequent creep behavior. *Int J Fatig* 2018;109:114–25. <https://doi.org/10.1016/j.ijfatigue.2018.01.001>.
- [96] Masuyama F, Nishimura N, Ozaki M. Creep properties of grade 91 castings and forgings with high residual elements. In: *Proceedings of the experience with creep-strength enhanced ferritic steels; 2004. San Diego, CA, USA, July 2004*.
- [97] Xu X, Siefert JA, Parker JD, Thomson RC. Localised creep cavitation on boron nitride in the heat affected zone of 9% Cr tempered martensitic steel welds. *Mater Des* 2020;196:109046. <https://doi.org/10.1016/j.matdes.2020.109046>.
- [98] Xu X, Siefert JA, Parker JD, Thomson RC. Influence of microstructure on cavitation in the heat affected zone of a Grade 92 steel weld during long-term high temperature creep. *Mater Character* 2020;170:110663. <https://doi.org/10.1016/j.matchar.2020.110663>.
- [99] Xu X. Microstructural evolution and creep damage accumulation in Grade 92 steel weld for steam pipe applications. PhD Thesis. Loughborough University; 2017. <https://hdl.handle.net/2134/25124>.
- [100] R5. *Assessment procedure for the high temperature response of structures*. Gloucester, UK: British Energy Generation Ltd; 2003. Issue 3.
- [101] Spindler M. The prediction of creep damage in type 347 weld metal. Part I: the determination of material properties from creep and tensile tests. *Int J Pres Ves Pip* 2005;82(3):175–84. <https://doi.org/10.1016/j.ijpvp.2004.09.003>.
- [102] Spindler M. The prediction of creep damage in Type 347 weld metal: Part II creep fatigue tests. *Int J Pres Ves Pip* 2005;82(3):185–94. <https://doi.org/10.1016/j.ijpvp.2004.09.004>. 2005.
- [103] Evans RW, Wilshire B. *Creep of metals and alloys*. 1985. United States. ISBN-10: 0904357597.
- [104] Yatomi M, O'Dowd NP, Nikbin KM, Webster GA. Theoretical and numerical modelling of creep crack growth in a carbon–manganese steel. *Eng Fract Mech* 2006;73:1158–75. <https://doi.org/10.1016/j.engfracmech.2005.12.012>.
- [105] Zhao L, Jing H, Han Y, Xiu J, Xu L. Prediction of creep crack growth behavior in ASME P92 steel welded joint. *Comput Mater Sci* 2012;61:185–93. <https://doi.org/10.1016/j.commatsci.2012.04.028>.
- [106] Zhang JW, Wang GZ, Xuan FZ, Tu ST. The influence of stress-regime dependent creep model and ductility in the prediction of creep crack growth rate in Cr–Mo–V steel. *Mater Des* 2015;65:644–51. <https://doi.org/10.1016/j.matdes.2014.09.070>.
- [107] Wen JF, Tu ST, Gao XL, Reddy JN. New model for creep damage analysis and its application to creep crack growth simulations. *Mater Sci Technol* 2014;30(1):32–7. <https://doi.org/10.1179/1743284713Y.0000000302>.
- [108] Song K, Zhao L, Xu L, Han Y, Hongyang Jing H. Experimental and numerical analysis of creep and damage behavior of P92 steel by small punch tests. *Theor Appl Fract Mech* 2019;100:181–90. <https://doi.org/10.1016/j.tafmec.2019.01.013>.
- [109] Zhang Y, Chen C, Jiang W, Tu S, Zhang X, Li F. Evaluation of the creep crack growth behavior in 9Cr–1Mo steel under different stress conditions. *Int J Pres Ves Pip* 2020;188:104174. <https://doi.org/10.1016/j.ijpvp.2020.104174>.
- [110] Zhao L, Xu L, Han Y, Jing H, Gao Z. Modelling creep-fatigue behaviours using a modified combined kinematic and isotropic hardening model considering the damage accumulation. *Int J Mech Sci* 2019;161:105016. <https://doi.org/10.1016/j.ijmecsci.2019.105016>. 162.
- [111] Hu J, Xuan F, Liu C. A void growth model of multiaxial power-law creep rupture involving the void shape changes. *Int J Mech Sci* 2018;144:723–30. <https://doi.org/10.1016/j.ijmecsci.2018.05.011>.
- [112] Manjoine MJ. Ductility indices at elevated temperature. *ASME J Eng Mater Technol* 1975;97(2):156–61. <https://doi.org/10.1115/1.3443276>.
- [113] Manjoine MJ. Creep-rupture behaviour of weldments. *Weld J* 1982;61:50–7 [research supplement].
- [114] Spindler MW. The multiaxial creep ductility of austenitic stainless steels. *Fatig Fract Eng Mater Struct* 2004;27:273–81. <https://doi.org/10.1111/j.1460-2695.2004.00732.x>.
- [115] Shingledecker JP, Pharr GM. The role of eta phase formation on the creep strength and ductility of INCONEL alloy 740 at 1023 K (750 °C). *Metall Mater Trans* 2012;43:1902–10. <https://doi.org/10.1007/s11661-011-1013-4>.
- [116] Isobe N, Yashirodai K, Murata K. Creep damage assessment for notched bar specimens of a low alloy steel considering stress multiaxiality. *Eng Fract Mech* 2014;123:211–22. <https://doi.org/10.1016/j.engfracmech.2014.01.017>. 123.
- [117] Zhang YC, Jiang W, Tu ST, Zhang XC, Ye YJ. Creep crack growth behavior analysis of the 9Cr–1Mo steel by a modified creep–damage model. *Mater Sci Eng* 2017;708:68–76. <https://doi.org/10.1016/j.msea.2017.09.112>.
- [118] Yatomi M, Nikbin KM. Numerical prediction of creep crack growth in different geometries using simplified multiaxial void growth model. *Mater A T High Temp* 2014;31(2):141–7. <https://doi.org/10.1179/1878641314Y.0000000008>.
- [119] Nikbin KM, Smith DJ, Webster GA. Prediction of creep crack growth from uniaxial creep data. *Proceedings of the Royal Society A* 1984;396:183–97.
- [120] Guo H, Ling C, Busso EP, Zhong Z, Li D. Crystal plasticity-based investigation of micro-void evolution under multiaxial loading conditions. *Int J Plast* 2020;129:102673. <https://doi.org/10.1016/j.ijplas.2020.102673>.

Raheeg is currently a PhD researcher at the composite research group, University of Nottingham (UK). She received the MSc degree (first class) in structural engineering from the University of Nottingham in 2018. She was awarded the EPSRC studentship to

pursue PhD in the field of high-temperature materials. Her current research involves investigating creep and creep-fatigue deformation mechanisms of advanced materials and alloys such as creep strength enhanced ferritic steels through a comprehensive theoretical, experimental and computational programme. She has published two papers in international peer reviewed journals and participated in international conferences.

Prof Jonathan is currently working as a Senior Technical Executive at the Electric Power Research Institute (EPRI) in the US. He is an international leading expertise on high temperature structural integrity assessment, materials characterisation and creep damage mechanics with rich experience working in both academia and industry. As Head of Department at University of Wales Swansea (UK), he was responsible for advanced collaborative research, training, and consultative programs involving companies in Europe, North America, the Far East and Australia as well as South Africa. He has authored or co-authored more than 60 major reports, over 200 peer reviewed publications and made over 80 invited presentations at Expert Workshops organized by Research Organizations, Universities, Government Agencies and at Bodies responsible for Codes and Standards.

Dr Ming is currently working as an assistant professor at the School of Mechanics, Civil Engineering and Architecture, Northwestern Polytechnical University. He obtained his PhD degree in mechanical engineering at the National University of Ireland, Galway in 2018. He is an author of more than 6 publications and conferences papers in the area of high-temperature materials, cyclic plasticity modelling, mechanical design and microstructure modelling for low carbon martensite steel. He was a visiting researcher at the Bernal Institute for micro-structure modelling of martensitic steel at University of Limerick and a research fellow at the University of Nottingham.

Dr Tao is currently an assistant professor in the department of Civil Engineering, University of Nottingham (UK). He has been working in numerical modelling on material/structural behaviours under extreme loadings as well as structural/material

micromechanics modelling and characterisation. He has extensive experience in modelling of the complex Multiphysics phenomena involved in material behaviour as well as assessment of material residual strength. His research also involves micromechanics of cellular materials, composite materials and bio-inspired materials. His work has been supported by DSTL, Royal Society, EPSRC and industrial partners. Dr Tao Liu has published over 30 referred papers in renown peer reviewed journals.

Prof Andy is an international leading expertise on high temperature structural integrity and failure analysis. His career extends over 35 years with experience on plant life assessment and extension, failure investigations, supporting generating sites and undertaking research in the Power Industry. He is a Visiting Professor in the Mechanical Engineering Department at Imperial College London and has been actively researching plant life assessment and condition monitoring methods for many years with UK universities and external research organisations. Andy has worked in both technical and managerial positions in the Power Industry, for many years as an external engineering consultant and currently for the plant operator as Chief Mechanical Engineer for EDF Energy; Coal, Gas and Renewables business. Prof Andy has published over 20 journal papers in international peer reviewed journals.

Prof. Wei Sun is an Emeritus Professor at the University of Nottingham who retired from the University in August 2020. Prof. Sun has been working in the areas of high temperature material behaviour and structural integrity for over 25 years. His research covers creep, thermomechanical fatigue and cyclic plasticity, miniaturized test methods etc. Research into fretting wear and damage, high temperature behaviour of coatings, welding process modelling, fracture of nuclear graphite, has also been carried out. He has published 250 journal articles and 160 conference contributions. He is a co-author of the book "Applied Creep Mechanics" (McGraw-Hill 2013). In the past 15 years, his research has been significantly supported by industrial organizations (including BF2RA, EDF and EPRI) and 7 EPSRC projects on conventional power plants. Prof Wei Sun is a member of HTMC of IoM.